Bayesian Multiple Extended Target Tracking Using Labeled Random Finite Sets and Splines

Abdullahi Daniyan, *Member, IEEE*, Sangarapillai Lambotharan, *Senior Member, IEEE*, Anastasios Deligiannis, *Member, IEEE*, Yu Gong, *Member, IEEE*, and Wen-Hua Chen, *Fellow, IEEE*

***Abstract*—In this paper, we propose a technique for the joint tracking and labeling of multiple extended targets. To achieve multiple extended target tracking using this technique, models for the target measurement rate, kinematic component, and target extension are defined and jointly propagated in time under the generalized labeled multi-Bernoulli filter framework. In particular, we developed a Poisson mixture variational Bayesian model to simultaneously estimate the measurement rate of multiple extended targets and extended target extension was modeled using B-splines. We evaluated our proposed method with various performance metrics. Results demonstrate the effectiveness of our approach.**

***Index Terms*—Multitarget tracking, extended target tracking, B-splines, variational Bayesian, Poisson mixture, random finite sets, RFS, labeled random finite sets, LMB, GLMB Bernoulli filter.**

I. Introduction

IN MULTI-TARGET tracking (MTT), the aim is to jointly estimate the number and state of multiple targets present within a tracking volume while maintaining target tracks/history (data association). This problem becomes even more challenging in the face of missed detections, false alarms and noisy or corrupted observations/measurements. The MTT problem can be addressed under a Bayesian formulation where models are used to relate unobserved states to measurements. A common representation of such models is to assume that one target produces one measurement per time step, e.g., see [1] and [2]. This is often referred to as the *standard* measurement or *point target* model.

However, with the increasing advances in sensor technology, the proliferation of high-resolution sensors (e.g., video cameras, phased array radars, ground or marine radar and laser range sensors) in recent years, size of the targets, or proximity between targets and sensor, can be such that the targets occupy multiple resolution cells of the sensor giving rise to more than one measurement per time step. Such targets are termed extended targets (ET). Therefore, the point target assumption does no longer hold in such scenarios. Scenarios where ETs may appear include using marine or ground radar to track sufficiently close ships or aeroplanes, using automotive radar for vehicle tracking or using laser range sensors for person tracking [3]. Besides, modern applications require extensive and detailed physical information about targets to achieve tasks including target detection, tracking, classification, recognition and identification. In such cases, the idea of ET becomes even more appealing and useful. Additionally, applications that require tracking a group of closely spaced targets in formation can benefit from the ET formulation [4]. This is because the knowledge of the size, shape, and orientation of the group formation can be crucial in practical applications where recognition and classification are of importance [4]. Hence, target extension model and other information (e.g., kinematics) for ETs are required for tracking application.

When considering ET measurement models, two main aspects are usually required and these are i) a model to describe the number of measurements generated by each ET; ii) a model to capture the target's spatial distribution. These two components however depend very much on the type of ET being tracked. For instance, a target (e.g., radar target) can generate measurements from different scatter points. Another target type may generate just a few observations around a scatter point [5]. In any case, we can consider the observations from an ET to be such that the detections are geometrically structured.

As for modelling the number of measurements generated by an ET, the authors in [6] and [7] proposed one such model where the number of ET measurements are modelled as an inhomogeneous Poisson distribution characterized by a rate parameter. Knowledge on the distribution of measurements and acquiring a good estimate of the measurement rate parameter especially in the case of spatially close extended targets are important to improve performance [8]. The work in [9] proposed a recursive Bayesian method with exponential forgetting factor to estimate the measurement rate. This method requires choosing an appropriate window size for the forgetting factor as this is application dependant.

With regards to modelling the target extent (i.e., shape and size) of an ET, this is possible even in the absence of a specific

Manuscript received November 10, 2017; revised April 12, 2018 and July 25, 2018; accepted September 14, 2018. Date of publication October 4, 2018; date of current version October 19, 2018. The associate editor coordinating the review of this manuscript and approving it for publication was Prof. François Desbouvries. This work was supported in part by the Engineering and Physical Sciences Research Council Grant EP/K014307/1, in part by the MOD University Defence Research Collaboration in Signal Processing U.K. and the Petroleum Technology Development Fund, Nigeria. *(Corresponding author: Abdullahi Daniyan.)*

A. Daniyan and W. H. Chen are with the Department of Aeronautical and Automotive Engineering, Loughborough University, Loughborough LE11 3TU, U.K. (e-mail: a.daniyan2@lboro.ac.uk; w.chen@lboro.ac.uk).

S. Lambotharan and Y. Gong are with the Signal Processing and Networks Research Group, Wolfson School of Mechanical, Electrical and Manufacturing Engineering, Loughborough University, Loughborough LE11 3TU, U.K. (e-mail: s.lambotharan@lboro.ac.uk; y.gong@lboro.ac.uk).

A. Deligiannis is with the Volvo Cars, Gothenburg 40531, Sweden (e-mail: anastasios.deligiannis@volvocars.com).

Color versions of one or more of the figures in this paper are available online at http://ieeexplore.ieee.org.

Digital Object Identifier 10.1109/TSP.2018.2873537

target structure. This can be achieved for example by methods including: i) assuming some general parametric shape such as an ellipse or a rectangle (see e.g., [4], [10]–[19]) or ii) assuming an arbitrary shape for the ET (see e.g., [20]–[27]). For the first approach mentioned (i.e., assuming a general parametric shape), the most common technique used is the random matrix method proposed in [10] where the ET extension was modelled as a symmetric positive definite matrix (i.e., the ET is assumed to be elliptical). This method has been applied in various scenarios in both LIDAR and marine radar tracking (see e.g., [28] and [29]). However, this method has limitations as its performance depends inherently on the elliptic shape assumption.

As for the approaches in [20]–[27], the ET shape is assumed to be arbitrary and the techniques used for the target extension can be summarized as star-convex based, Gaussian process based, multiple sub-ellipse based, extension deformation based and measurement generating points based. It is worth mentioning here that these methods were presented (for the most part) for single ET tracking. The star-convex method or its alternative, the Gaussian process model provides a systematic way to model different target shapes from ellipses [17] to arbitrary star-convex shapes [26]. However not all arbitrary shapes fit into the definition of star-convex shapes (where a set is called star-convex if each line segment from the center to any point is fully contained in the set). The multiple sub-ellipse based method [20], [24] models the extension of arbitrary ET shapes using multiple sub-objects (ellipses). These methods usually assume the number of sub-objects to be known. Choosing a suitable number of sub-ellipses may be a challenge especially when dealing with ETs whose true extension is not known or group targets whose formation change dynamically. The method in [22], involved estimating the shape of an ET using the PHD filter. The authors considered an augmented state representation of an extended target that consisted of linear and non-linear components. A spline was used to represent the measurement generating points on the boundary of a rectangle. The PHD filter was then applied for jointly estimating this target state. As for the extension deformation based approach, the authors in [21] considered an ET to have a reference extension with control points on its boundary and a deformed extension. Then some of the control points were aimed to be moved from the reference extension to the deformed extension. The authors assumed both the reference extension and the control points to be known. However, in practical applications where an ET has varying scattering points possibly due to sensor to target geometry, the number of control points can change.

Once the ET measurement model has been defined, a multi-object tracker can be implemented together with the ET measurement model to perform state and target number estimation under the Bayesian formulation. To achieve MTT in general, a number of algorithms have been proposed and used. The most widely applied methods are the global nearest neighbour (GNN) [2], [30], the joint probabilistic data association (JPDA) filter [2], multiple hypothesis tracking (MHT) [30], [31] and random finite set (RFS) based multi-target filters [32].

The GNN, JPDA and MHT techniques essentially rely on the same principle in that they basically keep multiple instances of single target filters for all possible objects. In other words, they require data association followed by single target filtering [33]. The RFS based methods however possess a desirable characteristic of avoiding data association and focus on filtering by seeking optimal and suboptimal estimates of the multi-target state [33].

Techniques for achieving ET MTT include use of the probability hypothesis density (PHD) filter (see e.g., [16], [28], [34]–[37]) and its cardinalized version the cardinalized-PHD (CPHD) filter (see e.g., [3], [38], [39]). The PHD filter recursively estimates the first order moment (intensity function) of a random finite set [32] while the CPHD filter, in addition to estimating the PHD of an RFS, estimates a truncated cardinality distribution. It provides a better cardinality estimate as compared to the PHD filter [40]. The cardinality-balanced multi-target multi-Bernoulli (CB-MeMBer) filter was proposed specifically to address the pronounced bias in the cardinality estimate of the MeMBer filter [32], [41]. The CB-MeMBer filter which is a recursion that propagates (approximately) the multi-target posterior density and is based on the assumption that every multi-target posterior is a multi-target multi-Bernoulli process is also RFS based and has been used in ET MTT (see e.g., [42], [43]). However, the PHD, CPHD and CB-MeMBer filters do not formally estimate target trajectories (i.e., perform data association) in their basic forms. A post processing step is required to achieve this. To alleviate this problem, the generalised labelled multi-Bernoulli (GLMB) filter [44] and it computationally efficient version the labelled multi-Bernoulli (LMB) filter [45] were proposed, all under the RFS framework. Both filters can in addition to recursively estimating the target state and the number of targets, provide track association histories (data association). Both filters have been used to achieve ET MTT [5] and [46].

It is therefore desirable to have an ET multi-target tracker capable of incorporating models of measurement rate and target extent into a tracker that can estimate extended target states, number of targets and maintain track association in order to achieve improved tracking performance. Recently, the authors in [5] and [46] proposed a method to achieve this through a recursive Bayesian rate estimator to compute the measurement rate of each target individually and sequentially. The authors used the random matrix approach to model the target extent and formulated expressions for achieving ET MTT under the framework of GLMB and LMB. This approach requires pre-setting a window size to perform the measurement rate estimation based on the rate estimation method proposed in [9]. The authors in [9] noted that the choice of the window size affects how fast or slow the estimated rate by their method changes to the true rate parameter. This requirement may mean parameter tuning to obtain the right window size in some applications. The ET extension model in this approach is restrictive in that not all ET can be modelled using the elliptical shape.

In this paper, we propose a multiple ET tracking technique using the framework of labelled random finite set. We refer to this technique as the ET generalised labelled multi-Bernoulli spline (ET-GLMB-S) filter. In our approach, we model the measurement rate of the ETs as a Poisson mixture and we use a Poisson mixture variational Bayesian (PMVB) to simultaneously

estimate the measurement rate of all ETs present. Based on [6], we model the target extent as a diffuse model of the measurement generating process such that the target extent is represented by a spatial probability distribution instead of modelling explicit measurement sources. We use B-splines to model this spatial probability distribution. We then employ our PMVB and spline approaches to the modified GLMB filter of [44] to achieve joint recursive estimate of ET state estimate, number of target and targets label tracking.

The main contributions of this paper in contrast with method proposed in [5], [46] are listed as follows. Firstly, we use a variational Bayesian based method to simultaneously estimate the measurement rate of targets present. Use of VB avoids explicitly pre-setting a window size and converges to the true rate parameter given the number of detections. This has the advantage of maximizing an explicit objective, and fast convergence in most cases. Secondly, we derive the lower bound for our variational Bayesian method to aid in monitoring convergence. Third, we use B-splines to model the target extent which will allow for more accurate modelling of targets with arbitrary extensions rather than the restrictive elliptical model of [5], [46]. Lastly, we describe the prediction and likelihood update equations for target extension under the B-spline model.

The remainder of the paper is organized as follows. In Section II, we provide some background information as well as define some notations and definitions used in the paper. Section III presents some background information on B-Splines. We introduce the proposed ET-GLMB-S filter along with related derivations in Section IV. We describe and derive our simultaneous measurement rate estimator, the PMVB in Section V. Section VI contains simulation results highlighting the performance of our proposed technique followed by concluding remarks in Section VII.

II. Background and Preliminaries

A. Multi-Target Bayes Filter

In Bayesian multi-target estimation, the aim is to recursively estimate at each time k (using two stages known as *prediction* and *update*) the state of multi-targets $X_k \subset \mathbb{X}$. With an RFS formulation, both the multi-target states X_k and multi-target observations $Z_k \subset \mathbb{Z}$ are modelled as RFS. A framework for dealing with RFSs is known as finite sets statistics (FISST) [32] which is based on the notion of integration/density that is consistent with point process theory [47].

In the *prediction* stage, the multi-target state at time $k-1$ is assumed to be distributed according to the density $\zeta_{k-1}(\cdot|Z_{1:k1})$, with $Z_{1:k-1}$ denoting an array of finite sets of measurements received up to and including time $k-1$. The multi-target prediction to time k given $k-1$ is given by the Chapman-Kolmogorov equation

$$\zeta_{k|k-1}(X_k|Z_{1:k-1}) = \int f_{k|k-1}(X_k|X)\zeta_{k-1}(X|Z_{1:k-1})\delta X, \quad (1)$$

where $f_{k|k-1}(\cdot|\cdot)$ is the multi-target transition kernel, and the integral is the set integral [32],

$$\int f(X)\delta X = \sum_{i=0}^{\infty} \frac{1}{i!} \int_{\mathbb{X}^i} f(\{x_1, \ldots, x_i\}) d(x_1, \ldots, x_i) \quad (2)$$

At time k, a new set of observations Z_k is available and modelled by a multi-target likelihood function $g_k(Z_k|X_k)$. Thus the *update* stage involves computing the multi-target posterior at time k given by Bayes rule

$$\zeta_k(X_k|Z_{1:k}) = \frac{g_k(Z_k|X_k)\zeta_{k|k-1}(X_k|Z_{1:k-1})}{\int g_k(Z_k|X)\zeta_{k|k-1}(X|Z_{1:k-1})\delta X}. \quad (3)$$

Both (1) and (3) above collectively form the multi-target Bayes filter. However, computing the exact multi-target posterior (i.e., (3)) is in general numerically intractable, and therefore approximations are required in order to derive practical algorithms [32]. One of such approximations is the RFS-based multi-object filters.

Earlier works on tractable RFS-based algorithms include the probability hypothesis density (PHD) filter [32], which propagates only the first moment of an RFS; the cardinalized PHD (CPHD) filter [48] which jointly propagates the probability distribution of the number of targets and the first order moment; the multi-target multi-Bernoulli (MeMBer) filter [32] and its cardinality-balanced version, the CMeMBer filter [41] which both propagate the multi-target posterior density. Although, both the (C)PHD and the (C)MeMBer RFS approaches do not require explicit data association, they do not maintain target labels over time (i.e., they instead perform multi-object filtering by providing a set of unlabelled point estimates at each time step as opposed to tracking). As a result of this, post-processing is required in applications to produce the tracks.

Recently, [44] and [49] propose the generalised labelled multi-Bernoulli (GLMB) filter which is an idea based on labelled-RFS to address the problem. In their approach, they assign distinct labels to each element of the target set, so that trajectory history of each object can be naturally identified, without the need for post-processing. The GLMB filter in [44] and [49] was for solving the multi-object tracking problem under the standard point-detection likelihood model (i.e., when targets generate at most one measurement per time step.) Furthermore, the works in [5] and [46] proposed a generalization of this idea to enable the GLMB filter to handle extended targets. In the subsequent sections, we propose an improved technique for handling extended targets based on this generalization under the labelled-RFS framework. Before proceeding to this, we introduce some definitions, notations and concepts as regards to labelled random finite sets.

B. Labeled Random Finite Sets

Notation 1: We use bold upper case letter ($\boldsymbol{X}$) and bold lower case letter ($\boldsymbol{x}$) to denote labelled sets and labelled vectors respectively. We adopt regular upper case letter (X) and regular lower case letter (x) for unlabelled sets and unlabelled vectors respectively.

Notation 2: For a real-valued function h, its multi-object exponential is

$$h^X \triangleq \prod_{x\in X} h(x) \tag{4}$$

with $h^{\emptyset} = 1$ by convention and the elements in set X can be of any type e.g., sets, scalars or vectors so long as the function $h(\cdot)$ accepts such arguments.

Notation 3: The generalized Kronecker delta function, and the set inclusion function are respectively defined as

$$\delta_Y(X) = \begin{cases} 1, & \text{if } X = Y \\ 0, & \text{otherwise,} \end{cases} \quad 1_Y(X) = \begin{cases} 1, & \text{if } X \subseteq Y \\ 0, & \text{otherwise,} \end{cases} \tag{5}$$

where both, X and Y can be of any type e.g., sets, scalars or vectors.

Definition 1: An RFS can be defined as a finite-set-valued random variable. The FISST notion of integration/density is used to characterize RFSs [32]. In an RFS, the number of points is random; the points themselves are random and unordered as opposed to a random vector.

Definition 2: A labelled RFS $\boldsymbol{X}$ with state space $\mathbb{X}$ and discrete label space $\mathbb{L}$, is an RFS on $\mathbb{X}\times\mathbb{L}$, such that the labels within each realization are always distinct. That is, if $\mathcal{L}(\boldsymbol{X})$ is the set of unique labels in $\boldsymbol{X}$, and the distinct label indicator function is defined as

$$\Delta(\boldsymbol{X}) = \begin{cases} 1, & \text{if } |\mathcal{L}(\boldsymbol{X})| = |\boldsymbol{X}| \\ 0, & \text{if } |\mathcal{L}(\boldsymbol{X})| \neq |\boldsymbol{X}|, \end{cases} \tag{6}$$

a labelled RFS $\boldsymbol{X}$ always satisfies $\Delta(\boldsymbol{X}) = 1$ [44], [49].

Definition 3: A generalized labelled multi-Bernoulli (GLMB) RFS is a labelled RFS with state space $\mathbb{X}$ and discrete label space $\mathbb{L}$, and is distributed according to [44], [49]

$$\zeta(\boldsymbol{X}) = \Delta(\boldsymbol{X}) \sum_{c\in\mathbb{C}} w^{(c)}(\mathcal{L}(\boldsymbol{X}))[p^{(c)}(\cdot)]^{\boldsymbol{X}}, \tag{7}$$

where $\mathbb{C}$ is a discrete index set, and $w^{(c)}(\mathcal{L})$ and $p^{(c)}(x,\ell)$ satisfy the following

$$\sum_{L\subseteq\mathbb{L}} \sum_{c\in\mathbb{C}} w^{(c)}(L) = 1, \tag{8a}$$

$$\int_{x\in\mathbb{X}} p^{(c)}(x,\ell)dx = 1. \tag{8b}$$

Definition 4: A labelled multi-Bernoulli (LMB) RFS is a cheaper approximation of the GLMB RFS. The LMB is a labelled RFS having a state space $\mathbb{X}$ and a discrete label space $\mathbb{L}$, which is distributed according to [45]

$$\zeta(\boldsymbol{X}) = \Delta(\boldsymbol{X}) w(\mathcal{L}(\boldsymbol{X}))[p(\cdot)]^{\boldsymbol{X}}, \tag{9a}$$

where

$$w(L) = \prod_{\ell\in\mathbb{L}} \left(1 - r^{(\ell)}\right) \prod_{\ell\in L} \frac{1_L(\ell) r^{(\ell)}}{1 - r^{(\ell)}}, \tag{9b}$$

$$p(x,\ell) = p^{(\ell)}(x), \tag{9c}$$

with $x \in X$ denoting e.g., a target state, $p^{(\ell)}(\cdot)$ and $r^{(\ell)}$ denoting the probability density and existence probability respectively of the track corresponding to label $\ell \in \mathbb{L}$.

III. B-Splines

In this section, we give a brief background on B-spline. For more details, refer to [50]–[52]. A B-spline is a piecewise polynomial function which can be used to represent a curve. Any arbitrary geometrical, numerical or statistical function can be described by the B-spline transformation [53]. One can control the shape of any curve by adjusting the locations of the control points. This movement can be on the entire curve in which case there is a global effect or on certain part of the curve (i.e., which will have a local effect) [54]. A key benefit of using B-spline is its local controllability. That is to say, by applying appropriate control point movements, a curve can be controlled locally. This feature is useful when approximating/modelling target extension from the multiple (and stochastic) measurements generated by the target. This feature is also useful in spline filter implementation [53].

Mathematically, a one-dimensional p-th order B-spline curve $\mathbb{S}(s)$ of degree $p-1$ of a curve parameter s can be defined as:

$$\mathbb{S}(s) = \sum_{i=1}^{n_p} \mathbb{P}_i \mathcal{B}_{i,p,\mathbf{t}}(s) \;\; 2 \le p \le n_p, \tag{10}$$

where $\mathbb{P}_i$ is the i-th control point, n_p denotes the total number of control points and $\mathbf{t}$ denotes a knot vector consisting of non-decreasing sequence of real valued numbers, where $\mathbf{t} = \{t_1, \ldots, t_r\}$, i.e., $t_i \le t_{i+1}, i = 1, \ldots, \tau$. The knot vector $\mathbf{t}$ relates the variable x to the control points [50]–[52]. The total number of knots is always greater than the total number of control points [50]. Adding or removing knots using appropriate control point movement can exactly replicate the function/curve, which is suitable for implementing filtering algorithms using splines [55], [56]. Also, a higher-order (three or more) B-spline curve tends to be smooth and maintains the continuity of the curve. The continuity of the B-spline curve enables continuous state estimation [55], [56]. The i-th B-spline basis functions of a variable s are denoted by $\mathcal{B}_{i,p,\mathbf{t}}(s)$ and defined as [50]–[52]:

$$\mathcal{B}_{i,1}(s) = \begin{cases} 1 & \text{if } t_i \le s < t_{i+1}, \\ 0 & \text{otherwise.} \end{cases} \tag{11}$$

$$\mathcal{B}_{i,p}(s) = \frac{s - t_i}{t_{i+p-1} - t_i} \mathcal{B}_{i,p-1}(s) + \frac{t_{i+p} - s}{t_{i+p} - t_{i+1}} \mathcal{B}_{i+1,p-1}(s) \tag{12}$$

where variables t_i denote knot elements; $\mathcal{B}_{i,p}(s)$ is non-zero in the interval $[t_i, t_{i+p}]$. The basis function $\mathcal{B}_{i,p}(s)$ can have the form $0/0$, in which case it assumes $0/0 = 0$ [52]. Furthermore,

$$\sum_{i=1}^{n_p} \mathcal{B}_{i,p}(s) = 1 \tag{13}$$

for any value of the parameter s. The basis functions are polynomials of degree $p-1$ [50], [52]. Moreover, a B-spline curve can be open, clamped or closed. An open B-spline curve is

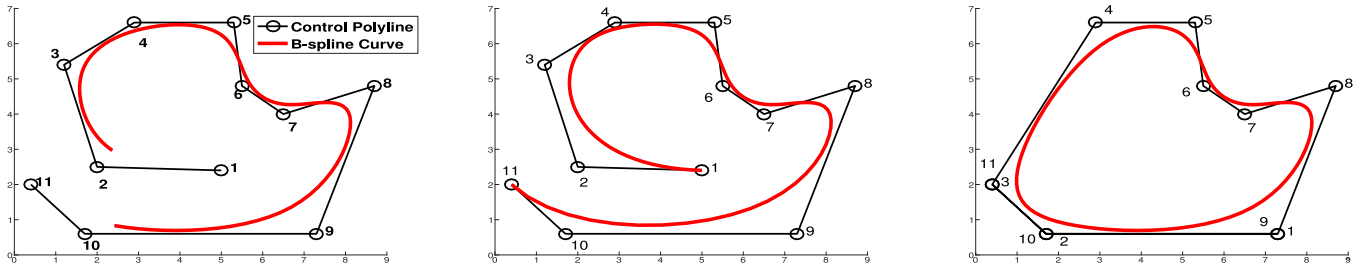

(a) Open spline. (b) Clamped spline. (c) Closed spline.

Fig. 1. Plots showing different constructions of B-splines. The control points are indicated by circles and numbered on the plots.

formed if the knot vector does not have any particular structure, hence the generated curve will not touch the first and last legs of the control polyline (see Fig. 1(a)). A B-spline is clamped when the curve is tangent to the first and the last legs of the control polyline (see Fig. 1(b)). This is achieved by repeating the first knot and the last knot $p+1$ times (i.e., of multiplicity $p+1$). A closed B-spline can be formed by repeating some knots and control points. In this case, the start and the end of the generated curve join together forming a closed loop (see Fig. 1(c)). This can be obtained by first designing a uniform knot sequence and then wrapping the first p and the last p control points. More specifically let $\mathbb{P}_1 = \mathbb{P}_{n_p-p+1}, \mathbb{P}_1 = \mathbb{P}_{n_p-p+2}, ..., \mathbb{P}_{p-2} = \mathbb{P}_{n-1}$ and $\mathbb{P}_{p-1} = \mathbb{P}_{n_p}$. Furthermore, unidimensional splines can be extended to multidimensional splines by using tensor product spline construction, see [50]. A spline subspace $\mathcal{B}_{i_j,p_j,\mathbf{t}_j}(s_j)$ is defined for each dimension where s_j denotes the variable in the j-th dimension. Thus, the spline representation of a multidimensional function $\mathbb{S}(s_1,\ldots,s_m)$ is given as

$$\mathbb{S}(s_1,\ldots,s_m) = \sum_{i_1}^{n_p}\cdots\sum_{i_m}^{n_p}\mathbb{P}_{i_1,\ldots,i_m}\,\mathcal{B}_{i_1,p_1,\mathbf{t}_1}(s_1)\cdots\mathcal{B}_{i_m,p_m,\mathbf{t}_m}(s_m). \quad (14)$$

The construction of the multidimensional spline polynomials above can be done by solving a corresponding set of linear equations [54], [55]. Moreover, the B-spline approach has been used in target tracking applications [53]–[56] in a continuous state space primarily because no special assumption on the noises is required, and it is able to accurately approximate arbitrary probability density or probability hypothesis density surfaces [54]. In most tracking algorithms, during the update stage, the states are updated, but in B-spline-based target tracking only the knots are updated [53], [55], [56].

IV. Multiple Extended Target Tracking With Labelled RFS and B-Splines

A. Problem Formulation

Consider an ET with scattering points along its boundary and within its body such that it generates measurements along its boundary and within its body. Let the labelled set of extended targets at time k be denoted by:

$$\boldsymbol{X}_k = \{(\mathfrak{x},\ell)_{i,k}\}_{i=1}^{|\boldsymbol{X}|} \triangleq \{\mathfrak{x}_{i,k}\}_{i=1}^{|\boldsymbol{X}|} \quad (15)$$

where $\ell \in \mathcal{L}(\boldsymbol{X})$ and $\mathcal{L}(\boldsymbol{X})$ is a set of unique labels in $\boldsymbol{X}$. $\mathfrak{x}_i$ is the labelled augmented state of the i-th target composed of the kinematic state, extension state and measurement rate parameter; we henceforth use $(\mathfrak{x},\ell)$ and $\mathfrak{x}$ interchangeably.

The set of observations received at time k is denoted

$$Z_k = \{z_{j,k}\}_{j=1}^{M_k}, \quad (16)$$

where M_k is the total number of measurements obtained at time k. The cumulative measurement sequence up to and including time k is $Z_{1:k} : Z_1, Z_2, \ldots, Z_k$. Note that the set Z includes both target originated measurements and measurements due to clutter. Each target, when present can generate one or more measurements. The measurements due to clutter are assumed to be Poisson distributed in number with rate parameter γ and having spatial distribution $\mathfrak{c}(\cdot)$. These clutter measurements are modelled as being uniformly distributed over the tracking scene. The goal at each time k is to estimate the labelled set of extended targets $\boldsymbol{X}_k$ given a set of corrupted observations Z_k.

B. Extended Target Observation Model

Here, we present the extended target observation model similar to [5] and [46]. At a given observation time, let the labelled RFS of multiple extended targets be $\boldsymbol{X} = \{\mathfrak{x}_1, ..., \mathfrak{x}_n\}$. Hence we assume that a particular target $\mathfrak{x} \in \boldsymbol{X}$ has probability of $p_D(\mathfrak{x})$ of being detected or misdetected with the probability $1 - p_D(\mathfrak{x})$. Furthermore, we assume that if the extended target $\mathfrak{x}$ is detected, it generates a set of measurements D with likelihood $g'(D|\mathfrak{x})$. Let $\mathfrak{D} = \{D_1, ..., D_d\}$ be the set of target detections. Then the set $\mathfrak{D}$ is distributed according to (see [32]):

$$g_{\mathfrak{D}}(\mathfrak{D}|\boldsymbol{X}) = \sum_{D_1 \uplus \cdots \uplus D_d = |\boldsymbol{X}|} \tilde{g}(D_1|\mathfrak{x}_1)\cdots\tilde{g}(D_{|\boldsymbol{X}|}|\mathfrak{x}_{|\boldsymbol{X}|}), \quad (17)$$

where $\tilde{g}(D|\mathfrak{x}_i)$ is an RFS distribution defined by

$$\tilde{g}(D|\mathfrak{x}_i) \propto \begin{cases} 1 - p_D(\mathfrak{x}) & \text{if } D = \emptyset, \\ p_D(\mathfrak{x})g'(D|\mathfrak{x}_i) & \text{otherwise.} \end{cases} \quad (18)$$

The symbol $\uplus$ denotes that the summation is taken over all mutually disjoint subsets of $\mathfrak{D}$, such that $D_1 \cup \cdots \cup D_{|\boldsymbol{X}|} = \mathfrak{D}$. Let the set $\mathfrak{K}$, which is independent of the target detections be a set of clutter observations and modelled as a Poisson RFS with rate γ and spatial distribution $\mathfrak{c}(\cdot)$, hence $\mathfrak{K}$ is distributed according to:

$$g_{\mathfrak{K}}(\mathfrak{K}) = e^{-\gamma}[\gamma\mathfrak{c}(\cdot)]^{\mathfrak{K}}. \quad (19)$$

Given the above, the set of multi-target observations, Z, is the union of the set of target detections and clutter observations, i.e., $Z = \mathfrak{D} \cup \mathfrak{K}$. Moreover, since $\mathfrak{D}$ and $\mathfrak{K}$ are independent, the multi-target likelihood is given by the convolution

$$g(Z|\boldsymbol{X}) = \sum_{\mathfrak{D} \subset Z} g_{\mathfrak{D}}(\mathfrak{D}|\boldsymbol{X}) g_{\mathfrak{K}}(Z - \mathfrak{D}) \tag{20a}$$

$$= \sum_{\mathfrak{D} \subset Z} g_{\mathfrak{D}}(\mathfrak{D}|\boldsymbol{X}) g_{\mathfrak{K}}(\mathfrak{K}). \tag{20b}$$

Furthermore, the multi-target likelihood can be expressed as a double summation over partitions of Z up to $|\boldsymbol{X}| + 1$, and mappings of measurement groups to targets as [5], [46]

$$g(Z|\boldsymbol{X}) = g_{\mathfrak{K}}(\mathfrak{K}) \sum_{i=1}^{|\boldsymbol{X}|+1} \sum_{\substack{\mathcal{W}(Z) \in \mathcal{P}_i(Z) \\ \theta \in \Theta(\mathcal{W}(Z))}} \left[\psi_{\mathcal{W}(Z)}(\cdot;\theta)\right]^{\boldsymbol{X}}, \tag{21a}$$

$$= e^{-\gamma} [\gamma \mathfrak{c}(\cdot)]^{Z} \sum_{i=1}^{|\boldsymbol{X}|+1} \sum_{\substack{\mathcal{W}(Z) \in \mathcal{P}_i(Z) \\ \theta \in \Theta(\mathcal{W}(Z))}} \left[\psi_{\mathcal{W}(Z)}(\cdot;\theta)\right]^{\boldsymbol{X}}, \tag{21b}$$

where $\mathcal{P}_i(Z)$ partitions Z into exactly i groups, and $\Theta(\mathcal{W}(Z))$ is the set of all one-to-one mappings $\theta : \mathcal{L}(\boldsymbol{X}) \rightarrow \{0, 1, \ldots, |\mathcal{W}(Z)|\}$ taking the labels in $\boldsymbol{X}$ to either a group of measurements in $\mathcal{W}(Z)$, or a misdetection. The term $\psi_{\mathcal{W}(Z)}(\mathfrak{x};\theta)$ is denoted as

$$\psi_{\mathcal{W}(Z)}(\mathfrak{x};\theta) = \begin{cases} 1 - p_D(\mathfrak{x}) & \theta(\ell) = 0, \\ \frac{p_D(\mathfrak{x}) g'(\mathcal{W}_{\theta(\ell)}(Z)|\mathfrak{x})}{[\gamma \mathfrak{c}(\cdot)]^{\mathcal{W}_{\theta(\ell)}(Z)}} & \theta(\ell) > 0, \end{cases} \tag{22}$$

where $\mathcal{W}_{\theta(\ell)}(Z)$ is the group of measurements in partition $\mathcal{P}_i(Z)$ that was assigned to label ℓ under the mapping θ, and $g'(D|\mathfrak{x})$ is the likelihood that a single extended target with labelled state $\mathfrak{x}$ generates measurement D. From (21b), it is quickly observed that computing $g(Z|\boldsymbol{X})$ requires summation over all partitions of the measurements, Z. This in general, will be numerically intractable because the sets of measurement partitions and group-to-target mappings can potentially become extremely large [5]. We discuss the idea of partitioning the measurement set Z next.

1) Measurement Set Partition: At time k, consider a set of measurements $Z_k = \{z_{1,k}, z_{2,k}, z_{3,k}\}$ as in Fig. 2. The Figure shows five possible partitions $\mathcal{P}_i(Z)$ of the set Z, with each partition containing non-empty cells $\mathcal{W}(Z)$. The index i represents the i-th partition i.e., $\mathcal{P}_i(Z)$. In each partition, say $i = 2$ (where there are two sub-groups/cells), the sub-groupings assumes that measurements in the same sub-group/cell belong to the same target or a clutter source.

Furthermore, the number of possible partitions grows as the size of the measurement set increases [8], [28]. Therefore, for a target tracking method to be computationally tractable, only a subset of the possible partitions needs to be considered [8], [28]. In addition, these subset of possible measurement partitions must represent the most likely of all partitions in order to achieve good tracking performance [8]. To this end, a number of techniques can be used such as a technique called distance partition was suggested by [8] and another technique namely subpartition algorithm was also proposed in [8] to better handle the case of spatially close targets. Two other methods for achieving feasible measurement set partitioning known as the predictive partition and the expectation maximization (EM) partition were also proposed in [28]. Moreover, the authors in [28] suggests that the distance partitioning, subpartition, prediction partition and EM (for Gaussian mixtures) partition can all be used together to achieve a feasible set of partition $\mathcal{P}_i(Z)$. Instead of using all three techniques as suggested by [28], we suggest that using the prediction partition of [28] with a variational Bayesian (VB) technique (for Gaussian mixtures) (see [57] chap. 10) suffices and offers improved performance in terms of computation. In the VB partition algorithm, the Gaussian mixture parameters are initialized with the means from the prediction partition method. These means include the means for both surviving and new born targets. The number of mixture components is set to either the maximum number of expected targets or the number of means from the prediction partition plus one. The extra added component is to capture the clutter measurements. Furthermore, using VB has the advantage of not knowing the number of clusters and does not suffer from singularity issues when compared to EM as highlighted in Chapter 10 of [57]. (see [57] chap. 10 for more details on VB for Gaussian mixtures.)

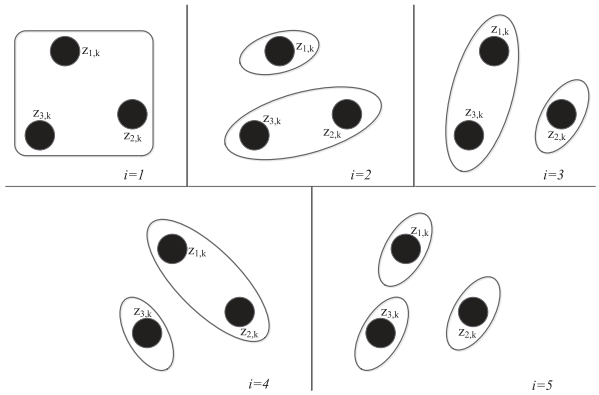

Fig. 2. Possible partitions of a set of three extended targets. Each black dot represent measurements. The index i represents the i-th partition. In each partition, say $i = 2$, the sub-groupings assumes that measurements in the same sub-group belong to the same target.

C. Extended Target State Model

We model the extended target state of the i-th target at time k with label ℓ as the tuple

$$\mathfrak{x}_{i,k} \triangleq (\lambda_{i,k}, x_{i,k}, \mathcal{X}_{i,k}) \tag{23}$$

where $\lambda_{i,k}$ is the Poisson measurement rate parameter, $x_{i,k}$ is the target kinematic state (such as position, velocity, acceleration) and $\mathcal{X}_{i,k}$ denotes the target extension/shape state. We model density of the rate parameter as a gamma distribution, the kinematic state as a Gaussian distribution and the extent as spatial probability distribution characterized by control points of a B-spline function. This spline is represented in the target state by the spline control points. Therefore, given the control points, we know the shape and size of the target. Conceptually,

the spline model can be used with random distribution models e.g., Gaussian, Poisson etc. However, given that the measurement model (as will be described in Section IV-C2) is Gaussian and the spline control points are a function of the measurements, there is an underlying Gaussian assumption in the pdf of χ used in our work.

Since only the i-th target is considered, we suppress the subscript i and the label ℓ from here on. The distribution of the extended target state is given by the density in (24). For simplicity, we henceforth adopt the notations for indices as $(\cdot)_{k-1}$, $(\cdot)_k$ and $(\cdot)_k^+$ to represent $(\cdot)_{k-1|k-1}$, $(\cdot)_{k|k-1}$ and $(\cdot)_{k|k}$ respectively.

$$p(\mathfrak{x}_{k-1}|Z_{1:k-1}) = p(\lambda_{k-1}|Z_{1:k-1})p(x_{k-1}|\mathcal{X}_{k-1}, Z_{1:k-1}) \times p(\mathcal{X}_{k-1}|Z_{1:k-1}). \quad (24)$$

We now describe the prediction and update stages of the extended target density of (24).

1) Prediction: We now compute the predicted density $p(\mathfrak{x}_k|Z_{1:k-1})$ of an extended target. To this end, we solve the Champan-Kolmogorov equation below:

$$p(\mathfrak{x}_k|Z_{1:k-1}) = \int f(\mathfrak{x}_k|\mathfrak{x}_{k-1})p(\mathfrak{x}_{k-1}|Z_{1:k-1})d\mathfrak{x}_{k-1} \quad (25)$$

where $f(\cdot|\cdot)$ denotes the transition density from time $k-1$ to k and $p(\mathfrak{x}_{k-1}|Z_{1:k-1})$ is the extended target density at time $k-1$. Next, let us assume the transition density can be written as

$$f(\mathfrak{x}_k|\mathfrak{x}_{k-1}) = f(\lambda_k|\lambda_{k-1})f(x_k|x_{k-1}, \mathcal{X}_k)f(\mathcal{X}_k|\mathcal{X}_{k-1}). \quad (26)$$

This equation assumes independence between the kinematic state $\mathfrak{x}_{k-1}$ and the extent state $\mathcal{X}_k$. This approximation is inherited from [10], where it was noted that this implies restrictions that can be justified in many practical applications [3], [46]. Relaxing this assumption will mean that χ_k is dependent on x_{k-1} which is a consideration for future work. Hence, the density of (25) yields

$$p(\mathfrak{x}_k|Z_{1:k-1}) = \int p(\lambda_{k-1}|Z_{1:k-1})f(\lambda_k|\lambda_{k-1})d\lambda_{k-1} \times \int p(x_{k-1}|\mathcal{X}_{k-1}, Z_{1:k-1})f(x_k|x_{k-1}, \mathcal{X}_k)dx_{k-1} \times \int p(\mathcal{X}_{k-1}|Z_{1:k-1})f(\mathcal{X}_k|\mathcal{X}_{k-1})d\mathcal{X}_{k-1}. \quad (27)$$

To solve for (27), similar to [9], we assume that the density of the measurement rate can be approximated as

$$\int p(\lambda_{k-1}|Z_{1:k-1})f(\lambda_k|\lambda_{k-1})d\lambda_{k-1} \approx \mathcal{GAM}(\lambda_k; \alpha_k, \beta_k),$$
$$\alpha_k = \frac{\alpha_{k-1}}{u}, \quad \beta_k = \frac{\beta_{k-1}}{u}, \quad (28)$$

where $\mathcal{GAM}(\lambda_k; \alpha_k, \beta_k)$ means λ_k is gamma distributed and governed by parameters α_k and β_k. The term $u > 0$ is a scaling term that ensures prediction such that the expected value of the rate parameter is retained and its variance is scaled (increased) by u. In our approach, choosing u such that it is positive suffices because the rate parameter converges to the true value when the PMVB is used.

The second line of (27) captures the kinematic component of the density. The kinematic density $p(x_{k-1}|\mathcal{X}_{k-1}, Z_{1:k-1}) = \mathcal{N}(x_{k-1}; m_{k-1}, P_{k-1} + \Sigma_{k-1})$ and under a linear Gaussian dynamic model, $f(x_k|x_{k-1}, \mathcal{X}_{k-1}) = \mathcal{N}(x_k; Fx_{k-1}, Q + \Sigma_{k-1})$. This has a closed form solution given by:

$$\int \mathcal{N}(x_{k-1}; m_{k-1}, P_{k-1} + \Sigma_{k-1})f(x_k|x_{k-1}, \mathcal{X}_{k-1})dx_{k-1} = \mathcal{N}(x_k; m_k, P_k + \Sigma_k),$$
$$m_k = Fm_{k-1}, \quad P_k = FP_{k-1}F^{\bar{T}} + Q. \quad (29)$$

where Σ_{k-1} denotes the covariance of control points.

The last component on the RHS of (27) (i.e., the last line) represents the extended target extension component which we assume to be a spatial probability distribution. We approximate this as

$$\int p(\mathcal{X}_{k-1}|Z_{1:k-1})f(\mathcal{X}_k|\mathcal{X}_{k-1})d\mathcal{X}_{k-1} \approx \mathbb{S}_k(\mathcal{X}_k; \mathbb{P}_k) \triangleq \mathbb{S}_k, \quad (30a)$$

where $\mathbb{S}_k$ is a d dimensional B-spline curve of order p, degree $p-1$, having knots $\mathbf{t}$ and characterized by control points $\mathbb{P}_k$. The B-spline curve $\mathbb{S}_k$ is given as:

$$\mathbb{S}_k = \sum_{j_1}^{N_k} \mathbb{P}_{k,j_1}\mathcal{B}_{i_1,p,\mathbf{t}}(s^{j_1}) \cdots \sum_{j_d}^{N_k} \mathbb{P}_{k,j_d}\mathcal{B}_{i_d,p,\mathbf{t}}(s^d), \quad (30b)$$

$$\mathbb{P}_k = F\mathbb{P}_{k-1} + w_{k-1}, \quad (30c)$$

where the subscript d in (30b) denotes the dimension of the control points, $\mathbb{P}_{k,j_d}$ denotes the vector of control points in the d-th dimension and N_k is the number of control points; w_{k-1} is an independent and identically distributed (i.i.d.) Gaussian noise vector with zero mean and covariance Σ_{k-1}. The B-spline used here is a closed spline which can be obtained as described in Section III. The spline has order $p = 4$ (degree 3). The knot elements are determined between intervals $[a, b]$ as [52]:

$$\mathbf{t} = \begin{cases} t_1, \ldots, t_p & = a \\ t_{i+p} & = a + \frac{i(b-a)}{N_k+p-1} \text{ for } i = 1, \ldots, (N_k - p) \\ t_{l-p}, \ldots, t_l & = b, \end{cases} \quad (30d)$$

where $l = N_k + p$.

The above gives the extended target predicted density $p(\mathfrak{x}_k|Z_{1:k-1}) \approx \mathcal{ETS}(\mathfrak{x}_k; \xi_k)$ where $\xi_k = (\alpha_k, \beta_k, m_k, P_k, \mathbb{S}_k, \mathbb{P}_k)$ is an array containing the predicted parameters which are defined by (28), (29) and (30a).

2) Update: When the set of measurements Z_k is available, each extended target needs to undergo measurement update using feasible subsets D of Z_k. We now describe the update procedure of a single extended target having a predicted density $\mathcal{ETS}(\cdot)$ given D. We assume that an extended target, when present and detected, generates measurements D and each element of D is generated according to the measurement model

$$\bar{z}_k = Hx_k + v_k \quad (31)$$

where matrix H is a transformation matrix and v_k is an i.i.d. Gaussian noise vector with mean zero and a covariance Σ_k; where Σ_k denotes the covariance of the control points.

Given the predicted density, we aim to use Bayes rule to compute the posterior density

$$p(\mathfrak{x}_k^+|Z_{1:k}) = \frac{p(\mathfrak{x}_k|Z_{1:k-1})g'(D|\mathfrak{x}_k)}{\int p(\mathfrak{x}_k|Z_{1:k-1})g'(D|\mathfrak{x}_k)d\mathfrak{x}_k} \tag{32}$$

We define the single target likelihood term $g'(D|\mathfrak{x}_k)$ of (32) in a similar manner to [10], [46] as

$$g'(D|\mathfrak{x}_k) = \mathcal{POIS}(|D|;\lambda_k)\prod_{j=1}^{|D|}\mathcal{N}(z_j;Hx_k,\Sigma_k) \tag{33}$$

so that the numerator of (32) is

$$\begin{aligned} &p(\mathfrak{x}_k|Z_{1:k-1})g'(D|\mathfrak{x}_k) \\ &\quad = \mathcal{GAM}(\lambda_k;\alpha_k,\beta_k)\mathcal{N}(x_k;m_k,P_k+\Sigma_k) \\ &\quad\times \mathbb{S}_k\mathcal{POIS}(|D|;\lambda_k)\prod_{j=1}^{|D|}\mathcal{N}(z_j;Hx_k,\Sigma_k). \end{aligned} \tag{34}$$

Note that the use of the spline representation in (34) does not mean that we take a spline to be a pdf. The spline representation in (34) rather is the pdf of the extent state, i.e., the pdf of the spline control points. Rearranging (34) yields

$$\begin{aligned} &= \mathcal{GAM}(\lambda_k;\alpha_k,\beta_k)\mathcal{POIS}(|D|;\lambda_k) \\ &\times \mathcal{N}(x_k;m_k,P_k+\Sigma_k)\prod_{j=1}^{|D|}\mathcal{N}(z_j;Hx_k,\Sigma_k) \\ &\times \mathbb{S}_k(\mathcal{X}_k;\mathbb{P}_k). \end{aligned} \tag{35}$$

where the first line captures the measurement rate component, the second line is the kinematic component and the last line is the extension component. From (35), given that the measurement rate component is independent of the extension and kinematic components, we can treat them separately.

As for the measurement rate component, we obtain the updated parameters α_k^+, β_k^+ and λ_k^+ using the Poisson mixture variational Bayesian (PMVB) technique which is described in details in Section V. The PMVB is initialized using the predicted α_k, and β_k as in (28), the mixture components C and the number of measurements from the ETs as obtained from the measurement partitioning technique of Section (IV-B1). The number of mixture components C can be set to the maximum expected number of components. Setting such a value for C, the VB model will not over fit the measurements to this number but rather converge to the true number of components present given the measurements. This is one of the advantages of the VB method over techniques such EM.

For the kinematic components, we have the update parameters given by the following:

$$\hat{z}_k = \frac{1}{|D|}\sum_{z_k\in D} z_k \tag{36a}$$

$$m_k^+ = m_k + K_k(\hat{z}_k - Hm_k) \tag{36b}$$

$$K_k = P_k H^T S_k^{-1} \tag{36c}$$

$$S_k = HP_kH^T + \frac{1}{|D|} \tag{36d}$$

$$P_k^+ = P_k - K_kHP_k \tag{36e}$$

$$\Sigma_k^+ = \frac{1}{|D|-1}\sum_{z_k\in D}(z_k-\hat{z}_k)(z_k-\hat{z}_k)^T \tag{36f}$$

As for the extension component, the number of control points are given as

$$N_k^+ = \begin{cases} |D|, & \text{if } |D|<\tau \\ \text{convx}(D), & \text{if } |D|>\tau, \end{cases} \tag{37}$$

where $\text{convx}(D)$ denotes those elements of D that form the convex polyline of the set of observations D and τ is a suitable threshold. We introduced the threshold τ to avoid using all the elements of D as control points particularly when $|D|$ and hence λ_k is large. This heuristic is based on the assumption that the ET has scattering points along its boundary (and within the body of the ET for an ET with large rate parameter λ_k). Applying this heuristic especially for a large λ_k would give the boundary outline of the ET. The control points are updated as

$$\mathbb{P}_k^+ = \begin{cases} \mathbb{P}_k + K_k(D - H\mathbb{P}_k), & \text{if } |\mathbb{P}_k| = |D| \\ (\mathbb{P}_k + K_k(D^a - H\mathbb{P}_k))\cup D^b, & \text{if } |\mathbb{P}_k| < |D| \end{cases} \tag{38}$$

where D^a and D^b are such that $D = D^a \cup D^b$. This means the detections D are split into two subsets D^a and D^b. The elements of D^a are elements in D with high association probabilities to $\mathbb{P}_k$ such that $|D^a| = |\mathbb{P}_k|$. This is achieved using the computationally attractive association method proposed in [58]. The control points update in (38) is akin to removal or addition of control points (and knots) in a B-spline. This translates to controlling the shape of the closed B-spline curve.

D. ET-GLMB Filter With B-Splines

Based on the proposed state space and measurement likelihood models presented above, we present the ET-GLMB filter with B-splines (ET-GLMB-S). The proposed ET-GLMB-S has two main stages (as is common to approximations of the Bayes multi-object filters), the prediction stage and the update stage. This is akin to respectively computing (1) and (3) of the Bayes multi-object filter. Using Notation 1, we rewrite (1) and (3) as:

$$\zeta_k(\boldsymbol{X}_k|Z_{1:k-1}) = \int f_k(\boldsymbol{X}_k|\boldsymbol{X})\zeta_{k-1}(\boldsymbol{X}|Z_{1:k-1})\delta\boldsymbol{X}, \tag{39a}$$

$$\zeta_k^+(\boldsymbol{X}_k|Z_{1:k}) = \frac{g_k(Z_k|\boldsymbol{X}_k)\zeta_k(\boldsymbol{X}_k|Z_{1:k-1})}{\int g_k(Z_k|\boldsymbol{X})\zeta_k(\boldsymbol{X}|Z_{1:k-1})\delta\boldsymbol{X}}. \tag{39b}$$

For the purpose of our derivation, we use the standard birth/death model similar to the one in [44] and [46] for the multi-target dynamics.

1) Prediction: For the prediction step, denote the probability of target survival and target death from present to next time as $p_S(\mathfrak{x},\ell)$ and $q_S(\mathfrak{x},\ell) = 1 - p_S(\mathfrak{x},\ell)$ respectively. The birth

density is an LMB having weight $w_B(\cdot)$, single target densities $p_B(\cdot,\ell)$ and a label space denoted by $\mathbb{B}_k$. Given that the multi-target posterior is a GLMB of the form (7) with label space $\mathbb{L}_{k-1}$, the predicted multi-target density at the next time step is the GLMB with label space $\mathbb{L}_k = \mathbb{L}_{k-1} \cup \mathbb{B}_k$ given by (see e.g., [44], [46])

$$\zeta_k(\boldsymbol{X}) = \Delta(\boldsymbol{X}) \sum_{c\in\mathbb{C}} w_k^{(c)}(\mathcal{L}(\boldsymbol{X})) \left[p_k^{(c)}(\cdot)\right]^{\boldsymbol{X}} \tag{40a}$$

$$w_k^{(c)}(L) = w_B(L-\mathbb{L}) w_S^{(c)}(L\cap\mathbb{L}), \tag{40b}$$

$$p_k^{(c)}(\mathfrak{x}_k,\ell) = 1_{\mathbb{L}}(\ell) p_S^{(c)}(\mathfrak{x},\ell) + (1-1_{\mathbb{L}}(\ell)) p_B(\mathfrak{x}_k,\ell), \tag{40c}$$

$$p_S^{(c)}(\mathfrak{x}_k,\ell) = \frac{\int p_S(\mathfrak{x}_k,\ell) f(\mathfrak{x}_k|\mathfrak{x}_{k-1},\ell) p^{(c)}(\mathfrak{x}_{k-1},\ell) d\mathfrak{x}_{k-1}}{\eta_S^{(c)}(\ell)}, \tag{40d}$$

$$\eta_S^{(c)}(\ell) = \int\int p_S(\mathfrak{x}_k,\ell) f(\mathfrak{x}_k \,|\, \mathfrak{x}_{k-1},\ell) \times p^{(c)}(\mathfrak{x}_{k-1},\ell) d\mathfrak{x}_{k-1} d\mathfrak{x}_k, \tag{40e}$$

$$w_S^{(c)}(J) = \left[\eta_S^{(c)}\right]^J \sum_{I\subseteq\mathbb{L}} 1_I(J) [q_S]^{I-J} w^{(c)}(I), \tag{40f}$$

$$q_S^{(c)}(\ell) = \int q_S(\mathfrak{x}_k,\ell) p^{(c)}(\mathfrak{x}_k,\ell) d\mathfrak{x}_k. \tag{40g}$$

2) Update: The update equations for the ET-GLMB-S filter is given in (41a)–(41c) shown at the bottom of this page, where

$$w_{\mathcal{W}(Z)}^{(c,\theta)}(L) = \frac{w^{(c)}(L)\left[\eta_{\mathcal{W}(Z)}^{(c,\theta)}\right]^L}{\sum_{c\in\mathbb{C}}\sum_{J\subseteq\mathbb{L}}\sum_{i=1}^{|J|+1}\sum_{\substack{\mathcal{W}(Z)\in\mathcal{P}_i(Z)\\ \theta\in\Theta(\mathcal{W}(Z))}} w^{(c)}(J)\left[\eta_{\mathcal{W}(Z)}^{(c,\theta)}\right]^J},$$

$$p^{(c,\theta)}(x,\ell\,|\,\mathcal{W}(Z)) = \frac{p^{(c)}(\mathfrak{x},\ell)\psi_{\mathcal{W}(Z)}(\mathfrak{x};\theta)}{\eta_{\mathcal{W}(Z)}^{(c,\theta)}(\ell)},$$

$$\eta_{\mathcal{W}(Z)}^{(c,\theta)}(\ell) = \int p^{(c)}(\mathfrak{x},\ell)\psi_{\mathcal{W}(Z)}(\mathfrak{x};\theta) d\mathfrak{x}, \tag{42}$$

with the term $\psi_{\mathcal{W}(Z)}(\mathfrak{x};\theta)$ given in (22).

The above prediction and update stages provide the ET-GLMB-S filter. Notice in both the prediction and update equations that the sum over $c\in\mathbb{C}$ is to facilitate the propagation of multiple hypotheses. These hypotheses involve different set of track labels which arise due to uncertainty in data association seen in the update stage of the Bayes multi-target filter [45]. Performing this can allow for a more accurate filtering process albeit at an increased computational effort. An efficient way will be to use just a single component (as in the Definition 4 above) to propagate the uncertainty of a single set of track labels. This can save on computational time but may sacrifice filtering accuracy. We call this method as the ET-GLMB-Sr filter.

V. The VB Model for Poisson Distributed Multiple Extended Target Measurements

In this section, we present a technique for jointly estimating the measurement rate per target for all targets using variational inference.

A. Context

Multiple extended targets under the measurement model of [6] and [7] are considered. It is assumed that the target's proximity to the sensor is such that the detections are geometrically structured. Furthermore, recall that the set of measurements at time k is a union of all target originated measurements and measurements due to clutter is given by (16). At time k, the number of measurements generated by the i-th target is a Poisson distributed random variable with rate parameter $\lambda_{k,i}$. The number of measurements due to clutter is assumed to be Poisson distributed with rate parameter γ_k. The set of measurements used to update the i-th target at time k is denoted as $Z_k^{(i)}$.[1] Let $\mathfrak{N}_k = \{N_1, N_2, \ldots, N_J\}$ be set of the number of measurements generated per extended target and $N_i = |Z_k^{(i)}|$. Using the measurement model of [7], each element of $\mathfrak{N}_k$ is Poisson distributed with rate parameter $\lambda_k^{(i)}$. We denote $\Lambda_k = \{\lambda_1, \lambda_2, \ldots, \lambda_J\}$ to be the set of rate parameters. Our goal is to jointly estimate at each time k, the measurement rates parameters which constitute of the elements of set Λ_k given $Z_{1:k}$ for each extended target. To this end, we present in Section V-B a recursive estimator of Λ_k using a PMVB technique.

[1] where $Z_k^{(i)} \equiv \mathcal{W}(Z)$ and $\mathcal{W}(Z)\in\mathcal{P}(Z); \mathcal{P}(Z) \angle Z_k$. The notation $\mathcal{P}(Z)\angle Z_k$ denotes the chosen partition of Z_k from all most likely feasible partitions $\mathcal{P}_i(Z)\ \forall i$ (Note that $\mathcal{P}_i(Z)\ \forall i$ includes other data associations with significant probabilities).

$$\pi(\boldsymbol{X}\,|\,Z) = \frac{\pi(\boldsymbol{X}) g(Z\,|\,\boldsymbol{X})}{\int \pi(\boldsymbol{X}) g(Z\,|\,\boldsymbol{X}) \delta\boldsymbol{X}} \tag{41a}$$

$$= \frac{\Delta(\boldsymbol{X}) g_C(Z) \sum_{c\in\mathbb{C}} \sum_{i=1}^{|\mathcal{L}(\boldsymbol{X})|+1} \sum_{\substack{\mathcal{W}(Z)\in\mathcal{P}_i(Z)\\ \theta\in\Theta(\mathcal{W}(Z))}} w^{(c)}(\mathcal{L}(\boldsymbol{X})) \left[\eta_{\mathcal{W}(Z)}^{(c,\theta)}(\cdot)\right]^{\mathcal{L}(\boldsymbol{X})} \left[p^{(c,\theta)}(\cdot\,|\,\mathcal{W}(Z))\right]^{\boldsymbol{X}}}{g_C(Z) \sum_{c\in\mathbb{C}} \sum_{L\subseteq\mathbb{L}} \sum_{i=1}^{|L|+1} \sum_{\substack{\mathcal{W}(Z)\in\mathcal{P}_i(Z)\\ \theta\in\Theta(\mathcal{W}(Z))}} w^{(c)}(L) \left[\eta_{\mathcal{W}(Z)}^{(c,\theta)}\right]^L} \tag{41b}$$

$$\pi(\boldsymbol{X}\,|\,Z) = \Delta(\boldsymbol{X}) \sum_{c\in\mathbb{C}} \sum_{i=1}^{|\boldsymbol{X}|+1} \sum_{\substack{\mathcal{W}(Z)\in\mathcal{P}_i(Z)\\ \theta\in\Theta(\mathcal{W}(Z))}} w_{\mathcal{W}(Z)}^{(c,\theta)}(\mathcal{L}(\mathbf{X})) \times \left[p^{(c,\theta)}(\cdot\,|\,\mathcal{W}(Z))\right]^{\boldsymbol{X}}. \tag{41c}$$

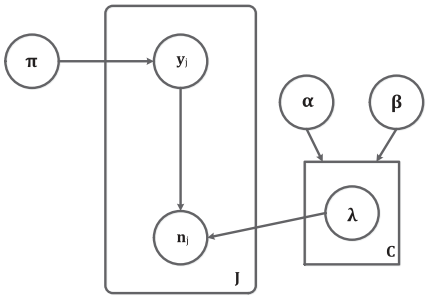

Fig. 3. Graphical model representation of the Poisson mixture model. n_j are observables which are governed by the Poisson distribution parameter λ. The latent variable y_j is a vector with a single component equal to 1 and the rest equal to 0, indicating cluster assignment of n_j. α, β are hyper-parameters of the Gamma distribution. π indicates the proportional of the components. J and C denote the number of observations and number of components respectively.

B. Poisson Mixture

In order to develop the PMVB model for our multiple extended target parameter estimation technique, we derive the mixture model equations for the Poisson distributed random variable. Fig. 3 shows the graphical representation of the PMVB model.

Suppose that the number of extended target measurements, Z_k, of Section V-A are independent and identically distributed (i.i.d.) and the observations are from a Poisson distribution with rate parameter $\lambda_{k,i}$. From here on, we omit the time index subscript k for ease of presentation. For each observable variable n_j, we have a corresponding latent variable $y_j \in Y$ (where $Y = \{y_1, y_2, \ldots, y_J\}$) is comprised of 1-of-$C$ binary vector with elements y_{jc} for $c = 1, \ldots, C$. The likelihood function of the Poisson distributed n is defined by

$$p(n|\lambda) = \frac{\lambda^n}{n!} e^{-\lambda} \tag{43}$$

Then the Poisson finite mixture is defined as:

$$p(n|\lambda, \pi) = \sum_{c=1}^{C} \pi_c p(n|\lambda_c) \tag{44}$$

where each Poisson density $p(n|\lambda_c)$ is a component of the mixture and has its own rate parameter λ_c; C denote total number of mixture components. π_c are the mixing coefficients with $0 \leq \pi_c \leq 1$ and $\sum_{c=1}^{C} \pi_c = 1$. The conditional distribution of the latent variables, Y, given the mixing coefficients, π, is defined as:

$$p(y|\pi) = \prod_{j=1}^{J} \prod_{c=1}^{C} \pi_c^{y_{jc}}. \tag{45}$$

The conditional distribution of the observation vectors given the component parameters and latent variables is

$$p(\mathfrak{N}|Y, \Lambda) = \prod_{j=1}^{J} \prod_{c=1}^{C} p(n_j|\lambda_c)^{y_{jc}}, \tag{46}$$

To simplify analysis, conjugate priors are used in Bayesian learning and therefore we choose the Dirichlet distribution for the mixing coefficients (see Chapter 10 of [57]) as

$$p(\pi) = \mathrm{Dir}(\pi|\mathfrak{a}_0) = \mathcal{C}(\mathfrak{a}_0) \prod_{c=1}^{C} \pi_c^{a_0 - 1}, \tag{47}$$

and a Gamma distribution for the rate parameters [59] as

$$p(\Lambda) = \mathrm{Gam}(\Lambda|\alpha, \beta) = \prod_{c=1}^{C} \frac{\beta^\alpha \lambda_c^{\alpha-1} e^{-\lambda_c \beta}}{\Gamma(\alpha)}, \tag{48}$$

where $\mathcal{C}(\mathfrak{a}_0)$ is the normalization constant for the Dirichlet distribution.

C. Variational Distribution

Given that the joint distribution of the observed data, latent variables and hidden parameters from Section V-B is

$$p(\mathfrak{N}, Y, \pi, \Lambda) = p(\mathfrak{N}|Y, \Lambda) p(Y|\pi) p(\pi) p(\Lambda); \tag{49}$$

the aim in variational learning is to find a variational distribution, $q(Y, \pi, \Lambda)$, on the latent variables and hidden parameters such that the variational lower bound $\mathcal{L}(q)$ given by

$$\mathfrak{L}(q) = \int \int q(Y, \pi, \Lambda) \ln \left\{ \frac{p(\mathfrak{N}, Y, \pi, \Lambda)}{q(Y, \pi, \Lambda)} \right\} d\pi d\Lambda, \tag{50}$$

is maximized or the Kullback-Leibler (KL) divergence given by

$$\mathrm{KL}(q||p) = -\int \int q(Y, \pi, \Lambda) \ln \left\{ \frac{p(Y, \pi, \Lambda|\mathfrak{N})}{q(Y, \pi, \Lambda)} \right\} d\pi d\Lambda, \tag{51}$$

is minimized. Note that maximizing the lower bound is equivalent to minimizing the KL divergence and the maximum of the lower bound occurs when the KL divergence vanishes and this occurs when $q(Y, \pi, \Lambda)$ equals the posterior distribution $p(Y|\mathfrak{N})$. $q(Y, \pi, \Lambda)$ is optimized in the set of probability distributions where the parameters are independent of each other. We factorize the variational distribution $q(Y, \pi, \Lambda)$ as

$$\begin{aligned} q(Y, \pi, \Lambda) &= q_1(Y) q_2(\pi, \Lambda) \\ &= q_1(Y) q_{\pi,2}(\pi) q_{\Lambda,2}(\Lambda) \end{aligned} \tag{52a}$$

The log of the optimized factors are:

$$\log q_1(Y) = \mathrm{E}_{q_1} [\log p(\mathfrak{N}, Y, \pi, \Lambda)] + \mathrm{const}_1 \tag{52b}$$

$$\log q_2(\pi, \Lambda) = \mathrm{E}_{q_2} [\log p(\mathfrak{N}, Y, \pi, \Lambda)] + \mathrm{const}_2 \tag{52c}$$

where const_1 and const_2 are normalization constants.

D. The Variational Learning

We recursively calculate (52b) and (52c) to perform the VB learning. From (52a), the optimal distributions for $q_\pi(\cdot)$ and $q_\Lambda(\cdot)$ are given by

$$q_\pi(\pi) = \mathrm{Dir}(\pi|\mathfrak{a}), \tag{53a}$$

$$q_\Lambda(\Lambda) = \prod_{c=1}^{C} \mathrm{Gam}(\lambda_c|\alpha, \beta) \tag{53b}$$

We compute the expectation step of our VB model using:

$$\log \rho_{jc} = \psi_0(a_c) - \psi_0\left(\sum_c^C a_c\right) + (\psi_0(\alpha_c) - \log \beta_c)\sum_{j=1}^J n_j - J\left(\frac{\alpha_c}{\beta_c}\right) - \sum_{j=1}^J \log(n_j!), \tag{54a}$$

with

$$r_{jc} = \frac{\rho_{jc}}{\sum_{c=1}^C \rho_{jc}} \tag{54b}$$

where $\psi_0(\cdot)$ is the digamma function (also known as the polygamma function of order 0) given by $\psi_0(a) = \frac{d}{da}\log\Gamma(a)$. The VB maximization step is computed using:

$$N_c = \sum_{c=1}^C r_{jc}, \qquad a_c = a_0 + N_c \tag{55a}$$

$$\alpha_c = \alpha_0 + \sum_{j=1}^J n_j, \quad \beta_c = \beta_0 + J \tag{55b}$$

$$\mathbb{E}[\lambda_c] = \frac{\alpha_c}{\beta_c} \qquad \mathrm{Var}(\lambda_c) = \frac{\alpha_c}{\beta_c^2} \tag{55c}$$

where N_c denotes the number of measurements generated up to now by a target with measurement rate λ_c. After PMVB step, the updated set of α_k^+ and β_k^+ are available as well as the set of the measurement rate, $\Lambda_k^+ = \{\lambda_1, \ldots, \lambda_C\}$ with $|\mathfrak{N}_k^+| = |\Lambda_k^+|$.

VI. Simulation Example

In this section, the performance of the proposed ET-GLMB-S and ET-GLMB-Sr filters are compared to the GLMB and random matrix based multiple extended target tracker of [46] which we refer to as the ET-GLMB-E filter. Additionally, we also compared the our approach with a filter we call the ET-GLMB-Em filter where we replaced the random matrix in [46] with the multiple sub-object method in [20].

A. Tracking Setup

We consider two different tracking scenarios. One scenario has four targets with different measurement rates and the other scenario has three targets also with different measurement rates. The dynamics of the target centroid is described using

$$x_k = Fx_{k-1} + w_k, \tag{56}$$

where x_k encapsulates the kinematic components i.e., position and velocity, $w_k \sim \mathcal{N}(0, Q_k)^T$ is a vector representing the process noise. The transition matrix F and the process noise covariance matrix Q_k are given as

$$F = \begin{bmatrix} 1 & \delta t \\ 0 & 1 \end{bmatrix} \otimes I_d, \quad Q_k = \sigma^2 \begin{bmatrix} \frac{\delta t^4}{4} & \frac{\delta t^3}{2} \\ \frac{\delta t^3}{2} & \delta t^2 \end{bmatrix} \otimes \Sigma_k \tag{57}$$

with the sample period $\delta t = 1$ and the process noise standard deviation is $\sigma = 2$ m/s^2. Furthermore, we set the probability of target survival to be $p_S = 0.99$. The initial gamma parameters used in the PMVB were set as $\alpha = 0.5$ and $\beta = 0.5$. The measurement rate threshold was set as $\tau = 20$.

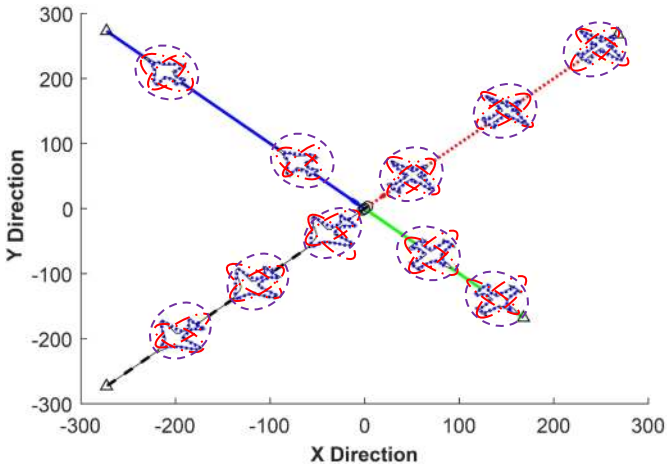

Fig. 4. Scenario I. True target trajectories (the straight lines) in the x-y plane with start/end (◯/△). The true target shape is shown in black line, our B-spline method in blue-dotted line, the multi-sub-object method in red-dash-dotted line and the random matrix method in purple-dashed line. All four targets start from the origin. The target plots shown are at intervals of 20 time steps.

B. Performance Metrics

We evaluate the performance of the proposed filter using filter run computation time (CT) and a metric based on the optimal sub-pattern assignment (OSPA) [60]. The OSPA metric used is similar to the modified (mOSPA) metric proposed in [3]. The mOSPA penalizes not only the cardinality and state estimations errors but also the measurement rate and extension errors. The main difference between our method and that in [3] is that we modified (45c) in [3] which was given as

$$d_{j,i}^{(c_X)} = \min\left(c_X, ||X_k^{(j)} - \hat{X}_{k|k}^{(i)}||_F\right) \tag{58a}$$

to read

$$d_{j,i}^{(c_\mathcal{X})} = \min\left(c_\mathcal{X}, \frac{1}{M}\sum^M \left|r\left(\mathcal{X}_k^{(j)}\right) - r\left(\hat{\mathcal{X}}_{k|k}^{(i)}\right)\right|^2\right). \tag{58b}$$

From (58a), X denotes the true positive semi-definite matrix capturing the target extension and $\hat{X}$ is its estimate; $||\cdot||_F$ denotes the Frobenius norm and the constant c_X is chosen so that it corresponds to the maximum expected error for the target extension state. From (58b), $\mathcal{X}$ denotes the true shape of the target and $\hat{\mathcal{X}}$ denotes its B-spline estimate; $r(\cdot)$ denotes a radial function that maps an angle to the radius of an arbitrary shape from its centroid (from 0 to 2π, M is the number of points $r(\cdot)$ was evaluated at) and it is convenient for representing and learning abstract shapes; $|\cdot|^2$ denotes the instantaneous error and $c_\mathcal{X}$ is chosen so that it corresponds to the maximum expected error for the target extension state. For brevity, we only present the section of the mOSPA metric for extended targets that differs from the one in [3]. Aside from this modification we have highlighted, all other aspects of the mOSPA are as in [3].

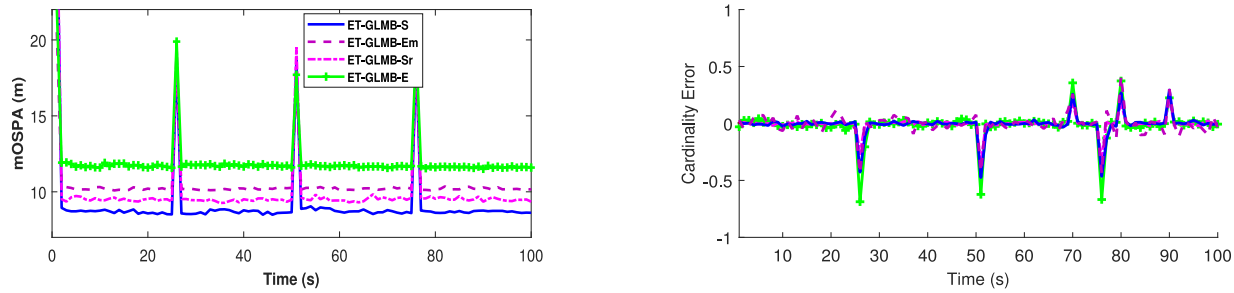

(a) (b)

Fig. 5. Scenario I: (a) mOSPA measure against time (b) Number of target estimation error against time. Results shown are for an average clutter rate of 20 Poisson clutter points per scan over 100 MC runs.

C. *Scenario I (where $\lambda_k < \tau$)*

In this scenario, four targets with measurement rates less than the measurement threshold are tracked in a $[-300, 300] \times [-300, 300]$ 2D surveillance area. The measurement rates and the time the targets enter and exit the tracking scene are given below:

$$\lambda_k^{(1)} = 5, \quad t_b^{(1)} = 1, \quad t_d^{(1)} = 70, \tag{59a}$$

$$\lambda_k^{(2)} = 10, \quad t_b^{(2)} = 26, \quad t_d^{(2)} = 80, \tag{59b}$$

$$\lambda_k^{(3)} = 15, \quad t_b^{(3)} = 51, \quad t_d^{(3)} = 90, \tag{59c}$$

$$\lambda_k^{(4)} = 20, \quad t_b^{(4)} = 76, \quad t_d^{(4)} = 100. \tag{59d}$$

This scenario lasts 100 time steps. The ground truth of the kinematic state of the targets are shown in Fig. 4. In this scenario, we considered two sub-objects for the ET-GLMB-Em filter.

In this scenario, we evaluate the performance of the proposed filter against the ET-GLMB-E and ET-GLMB-Em filters in terms of CT and mOSPA measure. Furthermore, since the targets enter and exist the scene at different times, we also evaluate the cardinality estimates of both filters. We assume that the clutter distribution is Poisson with uniform intensity. When evaluating the mOSPA measure and the cardinality, we considered a moderate clutter case where the average number of Poisson clutter points per scan is $\gamma_k = 50$. As for the CT performance evaluation, we considered three clutter cases. The first clutter has an average number of $\gamma_k = 30$ clutter points per scan with $pD = 0.8$, the second had $\gamma_k = 50$ with $pD = 0.9$ and the third case had $\gamma_k = 100$ clutter points per scan with $pD = 0.95$. The cardinality estimation is more challenging in the high clutter case.

The target extent estimate of the ET-GLMB-S filter (blue dotted line), the ET-GLMB-E (purple dash line) and ET-GLMB-Em (red dashed-dotted line) filters are shown in Fig. 4. The true target extent is shown in black line. As observed from the figure, the ET-GLMB-S filter is able to give a better estimate of the target extent, shape and orientation when compared to the other two methods. This improvement in the target extent estimation is due to our B-spline approach.

Fig. 5(a) depicts the averaged mOSPA measures for the filters over 100 Monte Carlo (MC) runs for the case where $\gamma_k = 50$. From the figure, it is observed that the ET-GLMB-S filter out performs the other three filters with the ET-GLMB-Em filter offering a similar level of performance to the ET-GLMB-Sr filter. The improved accuracy of the ET-GLMB-S filter when compared to the ET-GLMB-E filter is due to the proposed B-spline target extent model approach. The ET-GLMB-Em outperformed the ET-GLMB-E filter because it uses more the one ellipse to estimate the target extent and is therefore able to estimate the target extension better. The ET-GLMB-S filter offers a better tracking accuracy when compared to the ET-GLMB-Sr filter. This is because the implementation of the ET-GLMB-S filter includes multiple hypotheses propagation during the update stage of the filter. In Fig. 5(b), the cardinality errors of all four filters

TABLE I
FILTER PERFORMANCE COMPARISON IN TERMS OF COMPUTATION TIME (CT) FOR DIFFERENT PROBABILITY OF DETECTION p_D AND AVERAGE NUMBER OF CLUTTER POINTS γ_k

Filter	p_D, γ_k		
	0.8, 30	0.9, 50	0.95, 100
ET-GLMB-E	$6.65s$	$8.02s$	$9.83s$
ET-GLMB-Em	$6.90s$	$9.27s$	$10.15s$
ET-GLMB-Sr	$2.62s$	$3.11s$	$5.72s$
ET-GLMB-S	$6.93s$	$9.25s$	$10.11s$

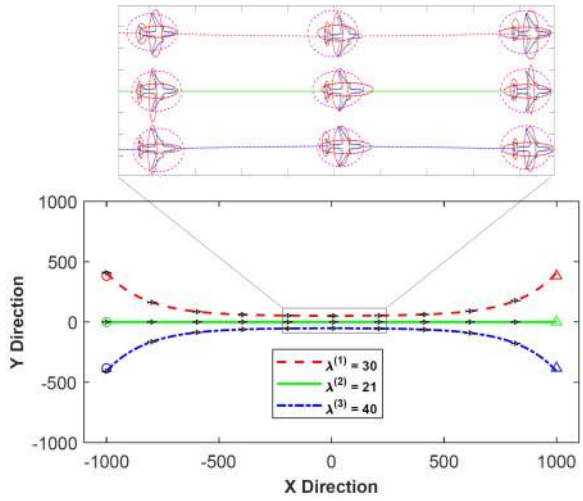

Fig. 6. Scenario II. In the top figure, the true target shape is shown in black line, our B-spline method in blue-dotted line, the multi-sub-object method in red-dash-dotted line and the random matrix method in pink-dashed line. All targets are simulated. The target plots shown are at intervals of 10 time steps.

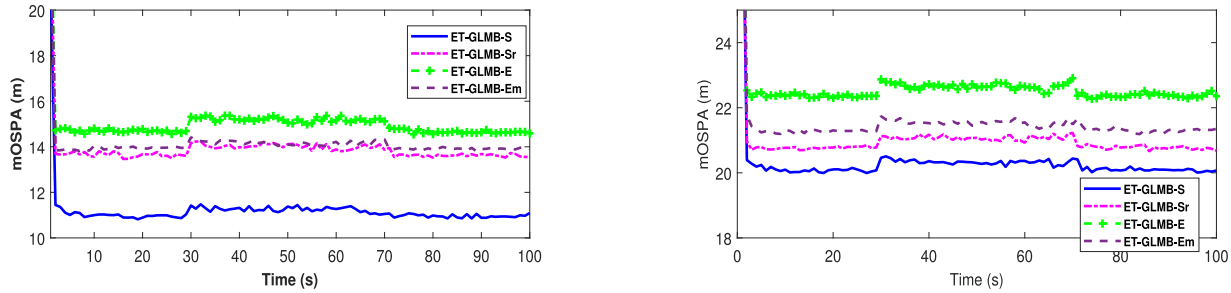

Fig. 7. Scenario II: (a) mOSPA measure against tracking time for $\gamma_k = 50$. (b) mOSPA measure against tracking time for $\gamma_k = 100$. Results shown are averaged over 100 MC trials.

are shown. This error measures the difference between the estimated and true number of multiple extended targets present to three decimal place. It can be seen that all four filters are able to estimate the cardinality of the targets with minimal error.

The results obtained for the CT of the filters for the three clutter rates and the different probability of detections for scenario I are presented in Table I. These are averaged over 100 MC runs. From the table, it is observed that the ET-GLMB-S filter and the ET-GLMB-Em filter have almost comparable CT. These two filters however take more time to compute when compared to the ET-GLMB-E filter for the scenario considered under the different p_D and γ_k settings. This is due mainly to the PMVB step required by the ET-GLMB-S filter to estimate the measurement rates for the targets as the lower bound computation in the PMVB step needs to converge in each iteration of the ET-GLMB-S filter. The ET-GLMB-Sr filter on the other hand gave the least CT when compared to the other two techniques despite the computation of the PMVB step. This is because the uncertainty of only a single set of track labels was propagated each time.

D. Scenario II (where $\lambda_k > \tau$)

For the second scenario, we considered the case where if $\lambda_k > \tau$, only the measurements that constitute of the convex hull of the targets are used in updating the control points of the spline. Therefore, in this scenario, we considered three closely spaced targets that enter and exit the tracking area at the same time but have different measurement rates. The measurement rates and the time instants the targets enter and exit the tracking scene are given below:

$$\lambda_k^{(1)} = 21, \quad t_b^{(1)} = 1, \quad t_d^{(1)} = 100, \tag{60a}$$

$$\lambda_k^{(2)} = 30, \quad t_b^{(2)} = 1, \quad t_d^{(2)} = 100, \tag{60b}$$

$$\lambda_k^{(3)} = 40, \quad t_b^{(3)} = 1, \quad t_d^{(3)} = 100. \tag{60c}$$

This scenario also lasts 100 time steps. The ground truth of the kinematic state of the targets are shown in the bottom plot of Fig. 6. The surveillance area is $[-1000, 1000] \times [-1000, 1000]$. In this scenario, we considered three sub-objects for the ET-GLMB-Em filter.

In this scenario, we highlight the performance of the filters under high clutter ($\gamma_k = 100$) conditions. We therefore focus on evaluating only the mOSPA measure and not the cardinality given that the number of targets are fixed during the entire time. Particularly, in this scenario, we highlight the performance of the filters in terms of their ability to track closely spaced targets. In this scenario, the three targets are in the closest proximity between time $k = 32$ and $k = 68$.

The target extent estimate of the ET-GLMB-S filter (blue dotted line), the ET-GLMB-E (purple dash line) and ET-GLMB-Em (red dashed-dotted line) filters are shown in . The true target extent is shown in black line. As observed from the figure, the ET-GLMB-S filter is able to give a better estimate of the target extent, shape and orientation when compared to the other two methods. This improvement in the target extent estimation is due to our B-spline approach.

Fig. 7 depicts the averaged mOSPA measures for the filters over 100 Monte Carlo MC runs for the case of low (Fig. 7(a)) and high (Fig. 7(b)) clutter rates respectively. In both figures, notice the increase in the estimation error in the ET-GLMB-Sr, ET-GLMB-Em and the ET-GLMB-E filters particularly during the times when all three targets are closest. This further highlights the drawback of the ET-GLMB-Sr filter where only the uncertainty of a single set of track labels is propagated during update of the filter.

Fig. 8 shows measurement rate estimation results obtained from applying the Bayesian rate estimation (BRE) used in [46] and our PMVB method to scenario II. In Fig. 8(a), a window size of 10 was used while a window size of 105 was used in 8(b) (for both methods). The estimated measurement rates appear to be noisy when a smaller window size is used for the BRE method (as observed from Fig. 8(a)). However, when a larger window size was used for the BRE method for the same problem, the estimation error reduces (see Fig. 8(b)). The proposed PMVB method however is less sensitive to the pre-set window size. Table II shows the root mean squared error (RMSE) computed for the two window size cases for both methods. It is observed that the RMSE for the PMVB relatively small for both cases. However, the RMSE for the BRE varied greatly for the BRE when different window sizes are used for the same application.

Overall, our proposed ET-GLMB-S filter has been shown to give improvement in terms of measurement rate and target extent

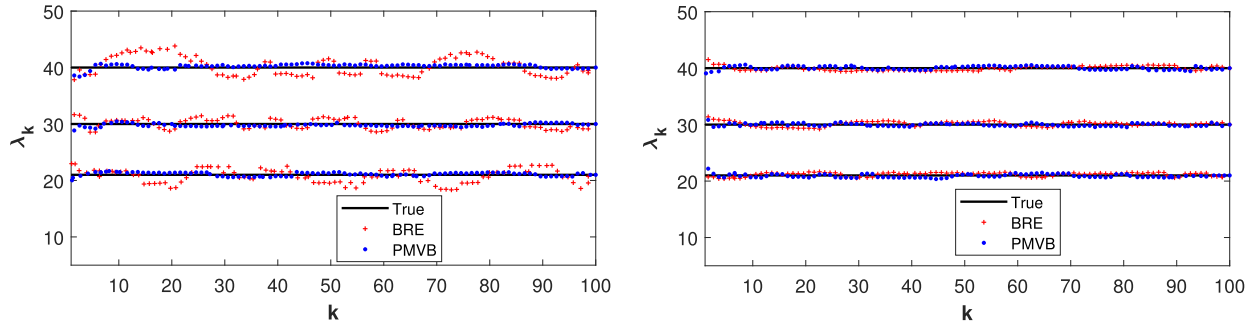

(a) Window size = 10

(b) Window size = 105.

Fig. 8. Plot showing Poisson rate parameter estimation results for the three measurement rates of Scenario II.

TABLE II
RMSE RESULT COMPARISON BETWEEN THE BRE AND THE PMVB METHODS

Method	RMSE	
	Window size = 10	Window size = 105
BRE	2.11	0.27
PMVB	0.29	0.26

estimation by giving a lower mOSPA measure when compared to the ET-GLMB-E and the ET-GLMB-Em filters. In addition, the ET-GLMB-Sr filter allows for an efficient implementation of the proposed technique as seen by the CT comparison.

VII. CONCLUSION

In this paper, we proposed an algorithm namely the ET-GLMB-S for the tracking of multiple extended targets in clutter. The algorithm was based on the labelled random finite sets framework which estimates multiple targets states and the number of targets while allowing continuous target tracks (labelling). The proposed algorithm in addition to estimating extended target kinematics also jointly estimates target measurement rate and extension. The main advantage of the proposed algorithms is the use of variational Bayesian approach to estimate measurement rates and the B-spline to model target extension. We performed simulation study to demonstrate the performance improvement offered by our method.

APPENDIX
VARIATIONAL LOWER BOUND DERIVATION

For the variational mixture of Poissons, the lower bound of (50) is given by

$$\mathfrak{L} = \sum_{Y} \int\int q(Y,\pi,\Lambda)\frac{p(\mathfrak{N},Y,\pi,\Lambda)}{q(Y,\pi,\Lambda)}d\pi\Lambda \tag{61a}$$

$$= \mathbb{E}[\log p(\mathfrak{N},Y,\pi,\Lambda)] - \mathbb{E}[\log q(Y,\pi,\Lambda)] \tag{61b}$$

where from (61b) above, we have:

$$\mathbb{E}[\log p(\mathfrak{N},Y,\pi,\Lambda)] = \mathbb{E}[\log p(\mathfrak{N}|Y,\Lambda)] + \mathbb{E}[\log p(Y|\pi)] + \mathbb{E}[\log p(\pi)] + \mathbb{E}[\log p(\Lambda)] \tag{61c}$$

and

$$-\mathbb{E}[\log q(Y,\pi,\Lambda)] = -\mathbb{E}[\log q(Y)] - \mathbb{E}[\log q(\pi)] - \mathbb{E}[\log q(\Lambda)] \tag{61d}$$

The various terms on the RHS of (61c) are:

$$\mathbb{E}[\log p(\mathfrak{N}|Y,\Lambda)] = \sum_{c=1}^{C} M_c \left(\mathbb{E}[\log \lambda_c] \sum_{j=1}^{J} n_j - J\mathbb{E}[\lambda_c] - \sum_{j=1}^{J} n_j! \right) \tag{62a}$$

$$\mathbb{E}[\log p(Y|\pi)] = \sum_{c=1}^{C}\sum_{j=1}^{J} r_{jc} \log \tilde{\pi}_c \tag{62b}$$

$$\mathbb{E}[\log p(\pi)] = \log \mathcal{C}(\mathfrak{a}_0) + (a_0 - 1)\sum_{c=1}^{C} \log \tilde{\pi}_c \tag{62c}$$

$$\mathbb{E}[\log p(\Lambda)] = \alpha_0 \log \beta_0 - \log \Gamma(\alpha_0) + \sum_{c=1}^{C} (\alpha_0 - 1)\mathbb{E}[\log \lambda_c] - \beta_0 \mathbb{E}[\lambda_c] \tag{62d}$$

where $\mathbb{E}[\log \lambda_c] = (\psi_0(\alpha_c) - \log \beta_c)$, $\mathbb{E}[\lambda_c] = \frac{\alpha_c}{\beta_c}$ and $\log \tilde{\pi}_c = \psi_0(a_c) - \psi_0(\sum_{c=1}^{C} a_c)$. Similarly, the terms on the RHS of (61d) are:

$$\mathbb{E}[\log q(Y)] = \sum_{c=1}^{C}\sum_{j=1}^{M} r_{jc} \log r_{jc} \tag{63a}$$

$$\mathbb{E}[\log q(\pi)] = \log \mathcal{C}(\mathfrak{a}) + \sum_{c=1}^{C} (a_c - 1)\log \tilde{\pi}_c \tag{63b}$$

$$\mathbb{E}[\log q(\Lambda)] = \sum_{c=1}^{C} (\alpha_c - 1)\psi_0(\alpha_c) + \log \beta_c - \alpha_c - \log \Gamma(\alpha_c). \tag{63c}$$

REFERENCES

[1] Y. Bar-Shalom and T. Fortmann, *Tracking and Data Association*, ser. Mathematics in Science and Engineering Series. New York, NY, USA: Academic, 1988.

[2] Y. Bar-Shalom, P. K. Willett, and X. Tian, *Tracking and Data Fusion*. Bradford, U.K.: Yorkshire Building Soc., 2011.

[3] C. Lundquist, K. Granstrm, and U. Orguner, "An extended target CPHD filter and a gamma Gaussian inverse Wishart implementation," *IEEE J. Sel. Topics Signal Process.*, vol. 7, no. 3, pp. 472–483, Jun. 2013.

[4] J. Lan and X. R. Li, "Tracking of extended object or target group using random matrix: New model and approach," *IEEE Trans. Aerosp. Electron. Syst.*, vol. 52, no. 6, pp. 2973–2989, Dec. 2016.

[5] M. Beard, S. Reuter, K. Granstrm, B. T. Vo, B. N. Vo, and A. Scheel, "A generalised labelled multi-bernoulli filter for extended multi-target tracking," in *Proc. 18th Int. Conf. Inf. Fusion*, Jul. 2015, pp. 991–998.

[6] K. Gilholm and D. Salmond, "Spatial distribution model for tracking extended objects," *Proc. Inst. Electr. Eng.–Radar, Sonar, Navigat.*, vol. 152, no. 5, pp. 364–371, Oct. 2005.

[7] K. Gilholm, S. Godsill, S. Maskell, and D. Salmond, "Poisson models for extended target and group tracking," in *Proc. Signal Data Process. Small Targets*, 2005, vol. 5913, pp. 230–241.

[8] K. Granström, C. Lundquist, and O. Orguner, "Extended target tracking using a gaussian-mixture PHD filter," *IEEE Trans. Aerosp. Electron. Syst.*, vol. 48, no. 4, pp. 3268–3286, Oct. 2012.

[9] K. Granström and U. Orguner, "Estimation and maintenance of measurement rates for multiple extended target tracking," in *Proc. 15th Int. Conf. Inf. Fusion*, Jul. 2012, pp. 2170–2176.

[10] J. W. Koch, "Bayesian approach to extended object and cluster tracking using random matrices," *IEEE Trans. Aerosp. Electron. Syst.*, vol. 44, no. 3, pp. 1042–1059, Jul. 2008.

[11] D. Angelova, L. Mihaylova, N. Petrov, and A. Gning, "A convolution particle filtering approach for tracking elliptical extended objects," in *Proc. 16th Int. Conf. Inf. Fusion*, Jul. 2013, pp. 1542–1549.

[12] H. Zhu, C. Han, and C. Li, "An extended target tracking method with random finite set observations," in *Proc. 14th Int. Conf. Inf. Fusion*, 2011, pp. 1–6.

[13] M. Schuster, J. Reuter, and G. Wanielik, "Probabilistic data association for tracking extended targets under clutter using random matrices," in *Proc. 18th Int. Conf. Inf. Fusion*, 2015, pp. 961–968.

[14] S. Reuter, B. Wilking, and K. Dietmayer, "Methods to model the motion of extended objects in multi-object Bayes filters," in *Proc. 15th Int. Conf. Inf. Fusion*, Jul. 2012, pp. 527–534.

[15] S. Reuter and K. Dietmayer, "Pedestrian tracking using random finite sets," in *Proc. 14th Int. Conf. Inf. Fusion*, 2011, pp. 1–8.

[16] K. Granstrm, S. Reuter, D. Meissner, and A. Scheel, "A multiple model PHD approach to tracking of cars under an assumed rectangular shape," in *Proc. 17th Int. Conf. Inf. Fusion*, Jul. 2014, pp. 1–8.

[17] M. Baum, B. Noack, and U. D. Hanebeck, "Extended object and group tracking with elliptic random hypersurface models," in *Proc. 13th Int. Conf. Inf. Fusion*, Jul. 2010, pp. 1–8.

[18] J. Degerman, J. Wintenby, and D. Svensson, "Extended target tracking using principal components," in *Proc. 14th Int. Conf. Inf. Fusion*, 2011, pp. 1–8.

[19] K. Granström, C. Lundquist, and U. Orguner, "Tracking rectangular and elliptical extended targets using laser measurements," in *Proc. 14th Int. Conf. Inf. Fusion*, 2011, pp. 1–8.

[20] K. Granström, P. Willett, and Y. Bar-Shalom, "An extended target tracking model with multiple random matrices and unified kinematics," in *Proc. 18th Int. Conf. Inf. Fusion*, 2015, pp. 1007–1014.

[21] X. Cao, J. Lan, and X. R. Li, "Extension-deformation approach to extended object tracking," in *Proc. 19th Int. Conf. Inf. Fusion*, Jul. 2016, pp. 1185–1192.

[22] C. Lundquist, K. Granstrm, and U. Orguner, "Estimating the shape of targets with a PHD filter," in *Proc. 14th Int. Conf. Inf. Fusion*, Jul. 2011, pp. 1–8.

[23] J. Lan and X. R. Li, "Tracking of extended object or target group using random matrix part ii: Irregular object," in *Proc. 15th Int. Conf. Inf. Fusion*, Jul. 2012, pp. 2185–2192.

[24] J. Lan and X. R. Li, "Tracking of maneuvering non-ellipsoidal extended object or target group using random matrix," *IEEE Trans. Signal Process.*, vol. 62, no. 9, pp. 2450–2463, May 2014.

[25] N. Wahlström and E. Özkan, "Extended target tracking using gaussian processes," *IEEE Trans. Signal Process.*, vol. 63, no. 16, pp. 4165–4178, Aug. 2015.

[26] M. Baum and U. D. Hanebeck, "Shape tracking of extended objects and group targets with star-convex RHMs," in *Proc. 14th Int. Conf. Inf. Fusion (FUSION)*, 2011, pp. 1–8.

[27] T. Hirscher, A. Scheel, S. Reuter, and K. Dietmayer, "Multiple extended object tracking using Gaussian processes," in *Proc. 19th Int. Conf. Inf. Fusion*, Jul. 2016, pp. 868–875.

[28] K. Granstrom and U. Orguner, "A PHD filter for tracking multiple extended targets using random matrices," *IEEE Trans. Signal Process.*, vol. 60, no. 11, pp. 5657–5671, Nov. 2012.

[29] K. Granstrm, A. Natale, P. Braca, G. Ludeno, and F. Serafino, "Gamma Gaussian inverse Wishart probability hypothesis density for extended target tracking using x-band marine radar data," *IEEE Trans. Geosci. Remote Sens.*, vol. 53, no. 12, pp. 6617–6631, Dec. 2015.

[30] S. Blackman and R. Popoli, *Design and Analysis of Modern Tracking Systems* (ser. Artech House radar library). Norwood, MA, USA: Artech House, 1999.

[31] S. S. Blackman, "Multiple hypothesis tracking for multiple target tracking," *IEEE Aerosp. Electron. Syst. Mag.*, vol. 19, no. 1, pp. 5–18, Jan. 2004.

[32] R. P. Mahler, *Statistical Multisource-Multitarget Information Fusion*. Norwood, MA, USA: Artech House, 2007.

[33] B.-N. Vo *et al.*, "Multitarget tracking," *Wiley Encyclopedia of Electrical and Electronics Engineering*, Sep. 2015.

[34] A. Swain and D. Clark, "The PHD filter for extended target tracking with estimable extent shape parameters of varying size," in *Proc.15th Int. Conf. Inf. Fusion*, Jul. 2012, pp. 1111–1118.

[35] A. J. Swain, "Group and extended target tracking with the probability hypothesis density filter," Ph.D. dissertation, Dept. Elect., Electron. Comput. Eng., Heriot-Watt Univ., Edinburgh, U.K., 2013.

[36] R. Mahler, "PHD filters for nonstandard targets, I: Extended targets," in *Proc. 12th Int. Conf. Inf. Fusion*, Jul. 2009, pp. 915–921.

[37] H. Zhang, H. Xu, X. Y. Wang, and W. An, "A PHD filter for tracking closely spaced objects with elliptic Random Hypersurface models," in *Proc. 16th Int. Conf. Inf. Fusion*, Jul. 2013, pp. 1558–1565.

[38] F. Lian, C. Han, W. Liu, J. Liu, and J. Sun, "Unified cardinalized probability hypothesis density filters for extended targets and unresolved targets," *Signal Process.*, vol. 92, no. 7, pp. 1729–1744, 2012.

[39] U. Orguner, C. Lundquist, and K. Granstrm, "Extended target tracking with a cardinalized probability hypothesis density filter," in *Proc. 14th Int. Conf. Inf. Fusion*, Jul. 2011, pp. 1–8.

[40] B.-T. Vo, B.-N. Vo, and A. Cantoni, "The cardinalized probability hypothesis density filter for linear Gaussian multi-target models," in *Proc. 40th Annu. Conf. Inf. Sci. Syst.*, 2006, pp. 681–686.

[41] B.-T. Vo, B.-N. Vo, and A. Cantoni, "The cardinality balanced multi-target multi-Bernoulli filter and its implementations," *IEEE Trans. Signal Process.*, vol. 57, no. 2, pp. 409–423, Feb. 2009.

[42] M. Liu, T. Jiang, and S. Zhang, "The sequential Monte Carlo multi-Bernoulli filter for extended targets," in *Proc. IEEE 18th Int. Conf. Inf. Fusion*, 2015, pp. 984–990.

[43] G. Zhang, F. Lian, and C. Han, "CB-MeMBer filters for nonstandard targets, I: Extended targets," in *Proc. IEEE 17th Int. Conf. Inf. Fusion*, Jul. 2014, pp. 1–6.

[44] B. T. Vo and B. N. Vo, "Labeled random finite sets and multi-object conjugate priors," *IEEE Trans. Signal Process.*, vol. 61, no. 13, pp. 3460–3475, Jul. 2013.

[45] S. Reuter, B. T. Vo, B. N. Vo, and K. Dietmayer, "The labeled multi-bernoulli filter," *IEEE Trans. Signal Process.*, vol. 62, no. 12, pp. 3246–3260, Jun. 2014.

[46] M. Beard, S. Reuter, K. Granstrm, B. T. Vo, B. N. Vo, and A. Scheel, "Multiple extended target tracking with labeled random finite sets," *IEEE Trans. Signal Process.*, vol. 64, no. 7, pp. 1638–1653, Apr. 2016.

[47] B.-N. Vo, S. Singh, and A. Doucet, "Sequential Monte Carlo methods for multitarget filtering with random finite sets," *IEEE Trans. Aerosp. Electron. Syst.*, vol. 41, no. 4, pp. 1224–1245, Oct. 2005.

[48] R. Mahler, "PHD filters of higher order in target number," *IEEE Trans. Aerosp. Electron. Syst.*, vol. 43, no. 4, pp. 1523–1543, Oct. 2007.

[49] B. N. Vo, B. T. Vo, and D. Phung, "Labeled random finite sets and the Bayes multi-target tracking filter," *IEEE Trans. Signal Process.*, vol. 62, no. 24, pp. 6554–6567, Dec. 2014.

[50] S. R. Buss, *3-D Computer Graphics: A Mathematical Introduction With OpenGL*. Cambridge, U.K.: Cambridge Univ. Press, 2003.

[51] D. F. Rogers, *An Introduction to NURBS: With Historical Perspective*. Amsterdam, The Netherlands: Elsevier, 2000.

[52] C. De Boor, *A Practical Guide to Splines*. New York, NY, USA: Springer, 2000.

[53] X. He, R. Sithiravel, R. Tharmarasa, B. Balaji, and T. Kirubarajan, "A spline filter for multidimensional nonlinear state estimation," *Signal Process.*, vol. 102, pp. 282–295, 2014.
[54] R. Sithiravel, M. McDonald, B. Balaji, and T. Kirubarajan, "Multiple model spline probability hypothesis density filter," *IEEE Trans. Aerosp. Electron. Syst.*, vol. 52, no. 3, pp. 1210–1226, Jun. 2016.
[55] R. Sithiravel, X. Chen, R. Tharmarasa, B. Balaji, and T. Kirubarajan, "The spline probability hypothesis density filter," *IEEE Trans. Signal Process.*, vol. 61, no. 24, pp. 6188–6203, Dec. 2013.
[56] K. Punithakumar, M. McDonald, and T. Kirubarajan, "Spline filter for multidimensional nonlinear/non-Gaussian Bayesian tracking," in *Proc. SPIE Defense Sec. Symp*. (International Society for Optics and Photonics), 2008, Paper 69 690K.
[57] C. Bishop, *Pattern Recognition and Machine Learning* (ser. Information Science and Statistics). New York, NY, USA: Springer, 2006.
[58] A. Daniyan, Y. Gong, and S. Lambotharan, "Game theoretic data association for multi-target tracking with varying number of targets," in *Proc. IEEE Radar Conf.*, May 2016, pp. 1–4.
[59] A. Gelman, J. B. Carlin, H. S. Stern, and D. B. Rubin, *Bayesian Data Analysis*, vol. 2. Boca Raton, FL, USA: CRC Press, 2014.
[60] D. Schuhmacher, B.-T. Vo, and B.-N. Vo, "A consistent metric for performance evaluation of multi-object filters," *IEEE Trans. Signal Process.*, vol. 56, no. 8, pp. 3447–3457, Aug. 2008.

Abdullahi Daniyan (S'13–M'18) received the B.Eng. (Hons.) degree in electrical and electronic engineering from the University of Bradford, Bradford, U.K., and the M.Sc. degree in signal processing, and the Ph.D degree in electronic, electrical and systems engineering from Loughborough University, Loughborough, U.K, in 2014 and 2018, respectively. He is currently a Research Associate with the Aeronautic and Automotive Engineering Department of Loughborough University, U.K. His research interests include multiple target tracking, Bayesian inference, Monte Carlo methods, particle filtering, sensor data fusion, machine learning, linear and nonlinear filtering, and estimation and renewable energy.

Sangarapillai Lambotharan (SM'06) received the Ph.D. degree in signal processing in 2017 from Imperial College London, London, where he remained until 1999 as a postdoctoral research associate. He was a visiting scientist with the Engineering and Theory Centre of Cornell University, USA in 1996. He is a Professor of Digital Communications and the Head of Signal Processing and Networks Research Group with the Wolfson School Mechanical, Electrical and Manufacturing Engineering, Loughborough University, Loughborough, U.K. Between 1999 and 2002, he was with Motorola Applied Research Group, U.K. and investigated various projects including physical link layer modeling and performance characterization of GPRS, EGPRS, and UTRAN. He was with Kings College London and Cardiff University as a Lecturer and Senior Lecturer, respectively, from 2002 to 2007. His current research interests include 5G networks, MIMO, radars, smart grids, machine learning, and network security. He has authored more than 200 journal and conference articles in these areas.

Anastasios Deligiannis (M'13) received the Diploma (Bachelor and Master's degrees equivalent) from the School of Electrical and Computer Engineering, University of Patras, Patras, Greece, in 2012, and the Ph.D. degree within the Signal Processing and Networks Research Group, Wolfson School of Mechanical, Manufacturing and Electrical Engineering, Loughborough University, Loughborough, U.K., in 2013, and the Ph.D degree in radar signal processing from Loughborough University, in 2016. From June 2016 to June 2018, he was as a Research Associate with Signal Processing, Loughborough University, U.K. Since June 2018, he is working with Volvo Cars as a radar performance engineer for autonomous driving projects. His research interests include signal processing algorithms, sparse array design, convex optimization and game theoretic methods, within the radar network framework, and wireless communications.

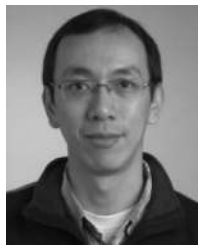

Yu Gong (M'07) has been with the School of Electronic, Electrical and Systems Engineering, Loughborough University, Loughborough, U.K., since 2012. He received the B.Eng. and M.Eng. degrees in electronic engineering from the University of Electronics and Science Technology of China, Chengdu, China, in 1992 and 1995 respectively, and the Ph.D. degree in communications from the National University of Singapore, Singapore, in 2002. After the Ph.D. graduation, he took several research positions in Institute of Inforcomm Research, Singapore and the Queens University of Belfast, Belfast, U.K., respectively. From 2006 and 2012, He had been a Lecturer with the School of Systems Engineering, University of Reading, U.K. His research interests include the area of signal processing and communications including wireless communications, cooperative networks, nonlinear and nonstationary system identification, and adaptive filters.

Wen-Hua Chen (M'00–SM'06–F'17) received the B.Eng. degree from Jiangsu University, Zhenjiang, China, in 1986, and the M.Sc. and Ph.D. degrees in control engineering from Northeastern University, Shenyang, China, in 1989 and 1991, respectively. He holds a Chair in Autonomous Vehicles with the Department of Aeronautical and Automotive Engineering, Loughborough University, Loughborough, U.K., where he is leading the Autonomous Systems Laboratory. He is also the Head of Control and Reliability Research Group. He has a considerable experience in control and signal processing and their applications in robots, aerospace, and automotive systems. He was a Lecturer and then an Associate Professor with the Department of Automatic Control, Nanjing University of Aeronautics and Astronautics, Nanjing, China, before moved to U.K. He was the Department of Aeronautical and Automotive Engineering, Loughborough University, in 2000 after having held a research position and then a Lecturer in control engineering with the Centre for Systems and Control, University of Glasgow, Scotland. He is a Chartered Engineer, the Institution of Mechanical Engineers and the Institution of Engineering and Technology, U.K. He has authored or coauthored more than 200 papers and 2 books.